

**Department of Physics and Astronomy
University of Heidelberg**

Bachelor Thesis in Physics
submitted by

Jan Philipp Klinger

born in Erbach i. Odw. (Germany)

2019

Spin Transport in Dipolar Gases

This Bachelor Thesis has been carried out by
Jan Philipp Klinger
at the
Kirchhoff-Institut in Heidelberg
under the supervision of
Prof. Thomas Gasenzer and Dr. Martin Gärttner

Abstract

In this work we numerically simulate the propagation of a single spin excitation placed in a two dimensional plane of a dipolar gas. The physical spread of this initially localized excitation is illustrated and its transport properties are investigated. The main emphasis is laid on observing Anderson localization and demonstrating the relation between Anderson localization and disorder. In order to distinguish Anderson localization from finite system effects, all propagations are simulated for different system sizes. As results we present a comparison between a localized and a delocalized expansion, caused by a different amount of disorder, as well as a connection between localization and the degree of randomness. Subsequently we will devote our attention to the energy eigenstates and their statistical properties. As before, we are interested in the localization behavior and investigate the extent of the eigenstates in different parts of the spectrum, as well as for different disorder.

Zusammenfassung

In dieser Bachelorarbeit simulieren wir die Ausbreitung einer einzelnen Spinanregung in einem zweidimensionalen, dipolaren Gas. Wir illustrieren die räumliche Ausdehnung der Anregung und untersuchen die Transporteigenschaften. Der Schwerpunkt dieser Arbeit liegt jedoch auf dem Aspekt der Anderson Lokalisierung. Vor allem möchten wir auf den Einfluss der Unordnung des Systems eingehen. Wir demonstrieren das Lokalisierungsverhalten, indem wir zunächst eine lokalisierte und eine delokalisierte Ausdehnung vergleichen. Dabei untersuchen wir die Expansion jeweils für verschiedene Systemgrößen, um Anderson Lokalisierung von möglichen Randeffekten, hervorgerufen durch unsere begrenzte Systemgröße, zu unterscheiden. Als Ergebnis präsentieren wir eine quantitative Verbindung zwischen Unordnung und Lokalisierung. Als letztes widmen wir uns den Energieeigenzuständen. Auch hier sind wir an dem Lokalisierungsverhalten interessiert und analysieren die räumliche Ausdehnung der Eigenzustände für verschiedene Bereiche des Spektrums, wie auch für verschiedene Unordnungen.

Contents

1	Introduction	1
1.1	Contents of this thesis	2
2	Rydberg Gas	3
2.1	Physical setup and assumptions	3
3	Concept of Anderson Localization	6
3.1	Generate randomness	8
3.2	Proving Anderson Localization	9
4	How to simulate spin transport	10
4.1	Hilbert space	10
4.2	Hamiltonian	10
4.2.1	Spin operators	11
4.2.2	Hopping Hamiltonian	12
4.3	Time evolution	13
4.3.1	Probability	14
4.4	Limitations	15
4.5	Disorder averaging	15
5	Transport properties	17
5.1	Mean square displacement	17
5.1.1	Diffusive processes	17
5.1.2	Mean square displacement of a quantum particle	18
5.2	Distribution width	18
5.3	Standard deviation	18
5.4	Participation ratio	20
5.5	Accumulated probability and radial density	22
6	Microscopic mechanism	23
6.1	Dressed states	24
6.2	Short distances	26
7	Numerical results: Transport behavior	28
7.1	Mean square displacement	29
8	Numerical results: Anderson Localization	31
8.1	Localization and density	32
8.1.1	Meeting the excitation at the edge	33
8.1.2	Distribution width	33
8.1.3	Participation ratio	34
8.1.4	MSD and MD	35
8.1.5	Localization length	36
8.2	Density dependency	38
8.2.1	Participation ratio	39
8.2.2	Distribution width	39
8.2.3	MSD and MD	40
8.2.4	Standard deviation	41

9 Energy eigenstates	42
9.1 Participation ratio	43
9.2 Level spacing	45
10 Conclusions	49
11 Outlook	50
References	52
Eidesstattliche Erklärung	54

List of Figures

1	Rydberg gas	4
2	Initial configuration	5
3	Single excitation	5
4	Finite size effects	9
5	Random configuration	16
6	Spin dynamics with 2 atoms	23
7	Ensemble with 8 atoms	24
8	Explaining a dressed state	25
9	Pair localization	26
10	Complexity of spin dynamics	27
11	Excitation in a system with 2000 atoms	28
12	Probability of finding the excitation far outside for a delocalized state	29
13	Mean square displacement	29
14	Localization effects in a system with 2000 atoms	31
15	Probability of finding the excitation far outside for a localized state	32
16	Comparing a localized and delocalized state: Probability curve	33
17	Comparing a localized and delocalized state: Distribution width	33
18	Comparing a localized and delocalized state: Participation ratio	34
19	Comparing a localized and delocalized state: MSD and MD	35
20	Comparing a localized and delocalized state: Standard deviation	36
21	Comparing a localized and delocalized state: Radial density	37
22	Density dependence: Participation ratio	39
23	Density dependence: Distribution width	39
24	Rescaling the arrangements	40
25	Density dependence: MSD and MD	40
26	Density dependence: Standard deviation	41
27	Comparing the population of eigenstates	42
28	Participation ratio for different energy eigenstates	43
29	Scheme of energy levels	45
30	Ratio of level spacings	46
31	Spectral density	47
32	Frequency of level spacing ratio	47
33	Mean level spacing ratio	48

Abbreviations

MSD	Mean square displacement
MD	Mean displacement
PR	Participation ratio
IPR	Inverse participation ratio
GOE	Gaussian orthogonal ensemble

1 Introduction

In this thesis we are going to explore the interplay between disorder and quantum transport.

The concept of quantum transport is relevant and interesting, not only from a purely academic standpoint, but also due to its direct applications in technological endeavors. For example, employing single molecules as active functional components in electronic devices constitutes a promising new technological concept of fast growing interest [1, 2]. Due to recent progress in the domain of electronic devices, we have reached the limits where quantum effects cannot be ignored anymore. This is not the only field, in which a better comprehension of the motion of quantum particles is crucial.

In particular, we are interested in quantum transport in a disordered network. In physics, as in everyday life, disorder describes some lack of regularity and often its inhomogeneities increase the complexity. Due to phenomena like Brownian motion, it appears that randomness is especially anchored in the microscopic world.

In this thesis we want to address a problem, which also only occurs in the microcosm: Anderson localization, which describes the absence of diffusion in a disordered quantum network. Caused by interference effects, this phenomenon depends on the degree of randomness and cannot be explained classically.

In order to investigate localization effects, a numerical simulation was developed, which allows the description of spin dynamics based on dipole-dipole interaction. This is motivated by the possibility to experimentally realize our setting in a Rydberg gas. Among others, we will explain specific behaviors on a microscopic level (< 10 atoms), as well as the diffusion of the excitation through a network at larger scale (10000 atoms).

We will examine the propagation through a disordered sample and discuss how this expansion depends on the magnitude of disorder. To generate the disorder most numerical approaches to the localization problem use a random distribution of on-site energies. Nevertheless, our disorder arises only through a random placement of the atoms. We will point out, why this results in a connection between the magnitude of the randomness and the density of the system.

On the one hand we will demonstrate with numerical results, how a different density (i.e. a different degree of randomness) can either lead to a localized or delocalized expansion. On the other hand we will try to find a quantitative dependency between the impact of the density and the extent of localization.

The goal of this thesis is to shed some light on the concepts of spin transport, and how simulations for such behavior can be treated numerically. As already mentioned, there will also be a focus on explaining the properties related to Anderson localization, especially its dependence on the degree of disorder.

1.1 Contents of this thesis

This thesis is intended to provide an insight into spin dynamics based on dipolar interaction $V(r) \propto \frac{1}{r^3}$, resulting in quite interesting phenomena like Anderson localization. The fundamental questions we address concerning the character of a single spin excitation are: Does the propagation behave like a random walk? Does the excitation move further and further away or does it remain close to its initial position?

We especially focus on the latter. In this thesis we wish to explain localization effects and possible influences on the localization length. In particular the density ρ attracts our attention and becomes an important quantity representing the degree of randomness and affecting the localization.

We start in chapter 2 with describing the physical setting of our dipolar gas and its properties. Both the dipole-dipole interaction and the Rydberg blockade radius is introduced. A brief review of Anderson localization is given in chapter 3. The simplest toy model for this kind of phenomenon, the Anderson tight binding model, is used to familiarize ourselves with the localization behavior and its criteria.

Chapter 4 is supposed to give an insight into how the numerical simulation was produced. First we start by giving an overview about our Hilbert space, followed by the dipolar XY spin Hamiltonian and the numerical solution of the Schrödinger equation. Main aspect of this chapter is to get to know the procedure of the time evolution and the calculation of the probability to find the excitation.

In chapter 5 important observables, that quantify spin transport are introduced.

First results are shown in chapter 6. By using a network with a small number of atoms (<10), which was manually created in a specific arrangement, the physical behavior of the spin interaction is illustrated. We point out and explain unexpected dynamics in order to prepare ourselves for systems with many more atoms.

In chapter 7 we use systems with up to 10.000 atoms to investigate the propagation of a single excitation placed in the center of our network. Measures like the mean square displacement help us to quantify the transport and to determine differences in the spread caused by varying Rydberg blockade radii.

The emphasis of this thesis is on detecting and explaining Anderson localization in our system as well as finding reasons for its appearance. Therefore we illustrate in chapter 8 basic differences between a localized and a delocalized excitation caused by a different density ρ . Subsequently we try to quantify this impact by establishing a link between the extent of localization and the density.

Last but not least I want to give a brief overview of the properties of the energy eigenstates in chapter 9. Quantities like the participation ratio are used to decide, whether a state is localized or not and how the extent of localization scales with the density.

2 Rydberg Gas

Rydberg atoms are one of the major platforms for realizing dipolar quantum gases [3]. Rydberg atoms are atoms with a single electron having a high principal quantum number [4]. Advantages are on the one hand the very high degree of experimental controllability due to advancements in laser cooling and on the other hand the enhanced polarizability and strong dipole-dipole coupling, caused by the far outside bounded electron [4, 5, 6]. Along with almost no radiative losses in Rydberg atoms, they can interact with each other for relatively long times and transport of excitations between many atoms becomes possible, even for extended time scales [5, 6, 7].

As one can see, especially due to the strong dipole-dipole coupling and the extended lifetime, a gas of Rydberg atoms offers an incredibly rich physical environment to observe excitation transport arising through dipole-dipole-interaction [5, 7]

In the following the details and simplifications of our framework are discussed.

2.1 Physical setup and assumptions

For the comprehension of this thesis it is not absolutely necessary to know the experimental details and realization of the spin transport. We rather use simplifications, which facilitate our work. Nevertheless we want to orientate ourselves as closely as possible to the experimental feasibilities. For that reason this work is inspired by the experimental results from the group of Matthias Weidemüller at the Physikalisches Institut. In their work [3], they investigated the relaxation of an isolated dipolar-interacting Rydberg quantum spin system by realizing a dipolar XY spin-1/2 model in an external field. We will make use of their theoretical description of spin dynamics as well as adapting experimental values.

We start from the assumption of dealing with a two dimensional gas of frozen Rydberg atoms. Frozen means, that we neglect any kind of movements, both thermal motion and motion caused by interaction of the particles. As a consequence the atoms are totally fixed at a certain position for the whole time.

The atoms' positions are randomly distributed within a circle of radius \mathcal{R} , which we call the system size from now on. Despite of the randomness we still consider a constant radial density.

Rydberg blockade

In the experiment one works with laser excitation to generate the Rydberg atoms. As a result the Rydberg blockade effect arises. This effect becomes important, when two Rydberg atoms are close enough. Due to their high polarization, they interact strongly, which leads to symmetric energy shifts [4, 5]. When the interaction is sufficiently large, the laser is out of resonance and only one atom at a time can be transferred to the Rydberg state [4, 7]. As a consequence each Rydberg-excited atom blocks further excitations within the blockade radius r_b [8]. The strength of the dipole blockade effect is externally tunable by using lasers with different linewidth [5]. That's why we will investigate, among others, the impact of different Rydberg blockade radii on the transport behavior. We will work with a Rydberg blockade radius in the region of $r_b = 2 - 10\mu m$.

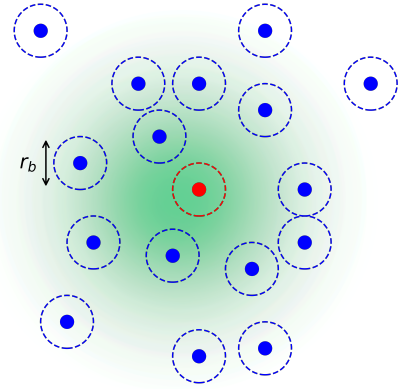


Figure 1: Rydberg gas with a single excitation

Interaction term

Because of the absent movements the only way the atoms can interact with each other is through long range effects. We introduce the interaction term V_{ij} , which gives the interaction between two atoms i and j . Depending on the kind of interaction, one wants to investigate, V_{ij} can vary. First, one differentiates between isotropic and anisotropic interaction. The main difference here is that the properties of isotropic interactions are the same in all directions, whereas in the anisotropic case quantities are direction dependent [9].

For isotropic hopping we define [9]:

$$V_{ij}^{Iso} = \frac{C}{|r_i - r_j|^\alpha} \quad (2.1)$$

And for anisotropic hopping [9]:

$$V_{ij}^{Aniso} = \frac{C(1 - 3 \cos^2(\theta_{ij}))}{|r_i - r_j|^\alpha} \quad (2.2)$$

where θ_{ij} is the angle between $|r_i - r_j|$ and the z-axis.

Because working in a two dimensional plane we assume that $\theta_{ij} = \frac{\pi}{2}$ and perform our calculations in case of isotropic hopping (2.1).

For $\alpha \leq d$ with dimension d , V_{ij} defines long-range hopping, otherwise one speaks about short-range hopping [9]. In particular we are interested in spin transport with its spin-spin-couplings based on the dipole-dipole-interaction. Due to its potential, which scales

with $\sim \frac{1}{|r|^3}$ we will investigate the case of $\alpha = 3$ [3].

In total we work with an isotropic short-range hopping interaction [3]:

$$V_{ij} = \frac{C}{|r_i - r_j|^3} \quad (2.3)$$

Single excitation

We are interested in the process of how an excitation travels through a system by jumping from site to site with considering only a single excitation. The setup can be illustrated by taking two different states into account [5, 3]:

$$|\downarrow\rangle = \left| nS_{\frac{1}{2}}, m_j = +1/2 \right\rangle \quad |\uparrow\rangle = \left| nP_{\frac{3}{2}}, m_j = +3/2 \right\rangle \quad (2.4)$$

The letter n labels the principal quantum number, S and P indicate the angular momentum and m_j denotes the atoms' fine structure. In the following we work with $|\uparrow\rangle$ and $|\downarrow\rangle$. The required interactions originate from the dipole-dipole interactions between pairs of atoms involving different combinations of $|\uparrow\rangle$ and $|\downarrow\rangle$ [3]. Note that we neglect any kind of relaxation processes (e.g. due to spontaneous decay). Therefore the total number of excitations is conserved and equals one throughout the experiment.

Figure (2) shows the initial situation of the experiment with N atoms in an unexcited state $|\downarrow\rangle$ for $t = 0$. Now our basic procedure is to place a single excitation $|\uparrow\rangle$ in the center of the 2D plane, illustrated in figure (3) and to study the behavior of the wave function for $t > 0$. For this, a simulation was implemented describing the propagation of such a single spin excitation under dipole-dipole interactions. In chapter 4, we will give insights in the simulation by presenting the calculation of the population, i.e. the probability of meeting the excitation on the particular atoms, for arbitrary time t as well as for $t \rightarrow \infty$.

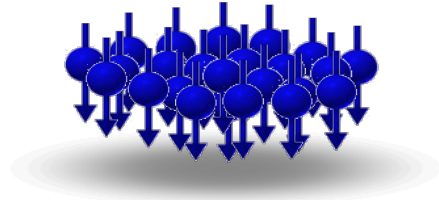


Figure 2: Initial configuration with N unexcited states

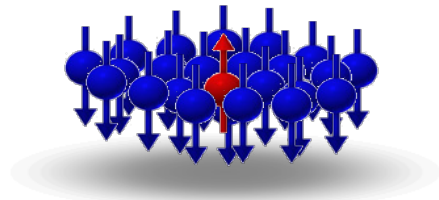


Figure 3: Start of the experiment by placing a single excitation in the center of the ensemble

3 Concept of Anderson Localization

When speaking about transport, we think about a movement from a point x to a point x' induced by an external force. In a classical transport setting, a particle moves. In quantum transport one propagates amplitudes, allowing for interference phenomena. Anderson localization is one of those effects caused by quantum interference.

Anderson localization describes the absence of diffusion of waves in a disordered medium [10]. It has its origin in the wave character of quantum particle propagation and results from interference of various components of the wave function scattered by randomly distributed fluctuations of the potential [11]. This phenomenon was first found by P.W. Anderson in 1958 and can be illustrated by considering a propagation of a quantum particle (e.g. electron) in a random potential [10]:

At the beginning $t = 0$ the electron is located in a certain small area of the sample. For increasing time, the electron wave function scatters off spatial inhomogeneities (spatial fluctuations of the potential) resulting in interference of multiple reflected components of the wave function [11]. As Anderson proved, this interference can restrict the propagation and its transport [10, 11]. It happens without interaction of particles and is therefore a one-particle phenomenon.

In the end one obtains (due to the randomness of the potential) a localized wave function, being zero outside of a certain area and decaying as a function of the distance from the center of the localization [11]. Consequently the probability to find the particle in its initial position is non-zero, even for $t \rightarrow \infty$ [11].

Based on the finite spatial extent similarities to the quantum bound state are recognizable. Note however, that the physical origin of the localization differs: a bounded particle is trapped in the potential well, whereas localization is caused by the interference of various components of the wave function scattered by randomly distributed fluctuations of the potential [11].

Due to the fact that Anderson localization arises from the wave description, this phenomenon can be applied to every kind of wave transport, like electromagnetic waves, acoustic waves, quantum waves, spin waves, etc [11].

In the following we introduce the original Anderson tight-binding model that represents the most simple toy model for studying localization effects. Primarily Anderson used it to present the electron propagation in the two-dimensional system with a random potential [10]. We use it to give a brief understanding of important impacts on transport behavior.

Based on the Schrödinger equation $i\hbar\frac{\partial}{\partial t}\Psi = H\Psi$ the model describes the evolution of a wave function Ψ on a d-dimensional lattice with N lattice sites. The Hamiltonian is given by:

$$(H\psi)(\bar{j}) = E_{\bar{j}}\psi(\bar{j}) + \sum_{\bar{k}\neq\bar{j}} V(|\bar{k} - \bar{j}|)\psi(\bar{k}) \quad (3.1)$$

For simplicity we assume nearest neighbor hopping with constant $V(r) = V$. $E_{\bar{j}} \in [-W, W]$ are randomly distributed on-site energies. W represents the strength of the disorder and V determines the hopping amplitude. Since V defines only the energy scale, our model can be characterized by only one parameter: the ratio W/V , which serves as a measure for the strength of the disorder [11].

We start by assuming a localized quantum particle at time $t = 0$ in the position \bar{r}_0 with the initial wave function $\Psi(\bar{r}_0, t = 0) = \delta(\bar{r} - \bar{r}_0)$. The propagation of this particle differs now quite a lot depending on the magnitude of disorder:

Without random disorder $W = 0$

Without disorder the electron will leave its specific place by diffusing to the neighboring sites and will occupy all sites of the lattice for $t \rightarrow \infty$. As a result the probability of meeting the electron in its original position equals almost 0 ($\sim \frac{1}{V_{volume}}$) [11].

With random disorder $W \neq 0$

Considering now disorder, one would intuitively think that the propagation depends on the strength of the disorder. Whereas sufficiently strong disorder should stop the propagation, very weak disorder is expected to not affect the diffusion [11]. In his original paper Anderson succeeded in deriving a dependency for a critical disorder strength W_c :

$$\frac{W_c}{V} = 2eK \ln(eK) \quad (3.2)$$

Accordingly the critical disorder W_c depends only on the lattice connectivity K (the number of nearest neighbor sites) [10, 11]. Anderson was not wrong, but it became apparent that the dimension d of the lattice is a more important parameter [12, 13, 11]. It could be shown that all states are localized in disordered systems with dimension $d \leq d_c = 2$ [13, 14, 15].

Summarized:

The diffusion is abolished and the particle/excitation remains localized, if:

- $d \leq 2$ and W is arbitrary
- $d \geq 3$ and W is sufficiently large

Note, that this is only valid, if the couplings V_{ij} at large distances R decay faster than R^{-d} , then (for $d \leq 2$) all states are localized and diffusive transport does not occur [10, 9, 7]. As a consequence there has to be localization effects observable in terms of our setting, since we assume a 2D ensemble of atoms with a dipole-dipole interaction $\approx R^{-3}$.

Nevertheless we still need a criterion whether a particle is localized or not. In order to speak of localization the mean displacement has to stay below a certain constant C uniformly in time [16, 11]:

$$\sum_{n \leq N} |\Psi(t, n)|^2 \cdot |r_n^-| < C \quad \forall t > t' \quad (3.3)$$

As requirement for eq. (3.3) the wave function has to decay sufficiently fast, meaning an exponential decrease (or at least polynomial with $|\Psi| < r^\alpha$ and $\alpha < -\frac{d}{2}$) as a function of distance from its center \bar{x}_0 [17, 18, 13, 14, 19]. In case of the exponential decay rate the wave function scales like:

$$\Psi(\bar{x}) \propto \exp\left(-\frac{|\bar{x} - \bar{x}_0|}{\xi}\right) \quad (3.4)$$

ξ is called the localization length [18].

3.1 Generate randomness

As should be evident now, localization is caused by the randomness of the potential [10]. Using the standard tight-binding Anderson Hamiltonian (3.1) with on-site potential disorder, is one of the easiest and most used numerical approaches to the localization problem.

Nevertheless we won't follow this approach. We won't consider a lattice, with randomness arising through the on-site disorder. This was already done in different researches [20, 19], where mostly the impact of the magnitude of on-site disorder or of the vacancy concentration in a lattice were investigated.

We consider the case in which the on-site potential is for every atom the same, i.e. we can drop it. The needed randomness occurs only from the randomness of the atom placement. While low densities corresponds to highly random arrangements, high densities form a more ordered system. A lattice would result in a perfectly ordered system with 0 randomness. Therefore by identifying randomness with the density, one would intuitively expect localization effects rather for low densities than for high densities. Answering this question of the relation between appearance of localization and the density of the ensemble is one of the goals of this thesis.

3.2 Proving Anderson Localization

The theory states, that there has to be localization in 2D regardless of the randomness [11]. Numerically this is hard to prove.

By definition, Anderson localization occurs if the mean displacement (3.3) doesn't increase above a certain threshold C . Unfortunately this case appears as well, when the expansion of the excitation reaches the boundaries due to finite size effects. The problem is, once the excitation reaches the boundaries, there could be no localization, or the localization length is larger than the system size. For being able to certainly claim whether an excitation is localized, the expansion has to stop before the boundaries. To distinguish those two scenarios we calculate the mean displacement for increasing number of atoms and system size at a fixed density.

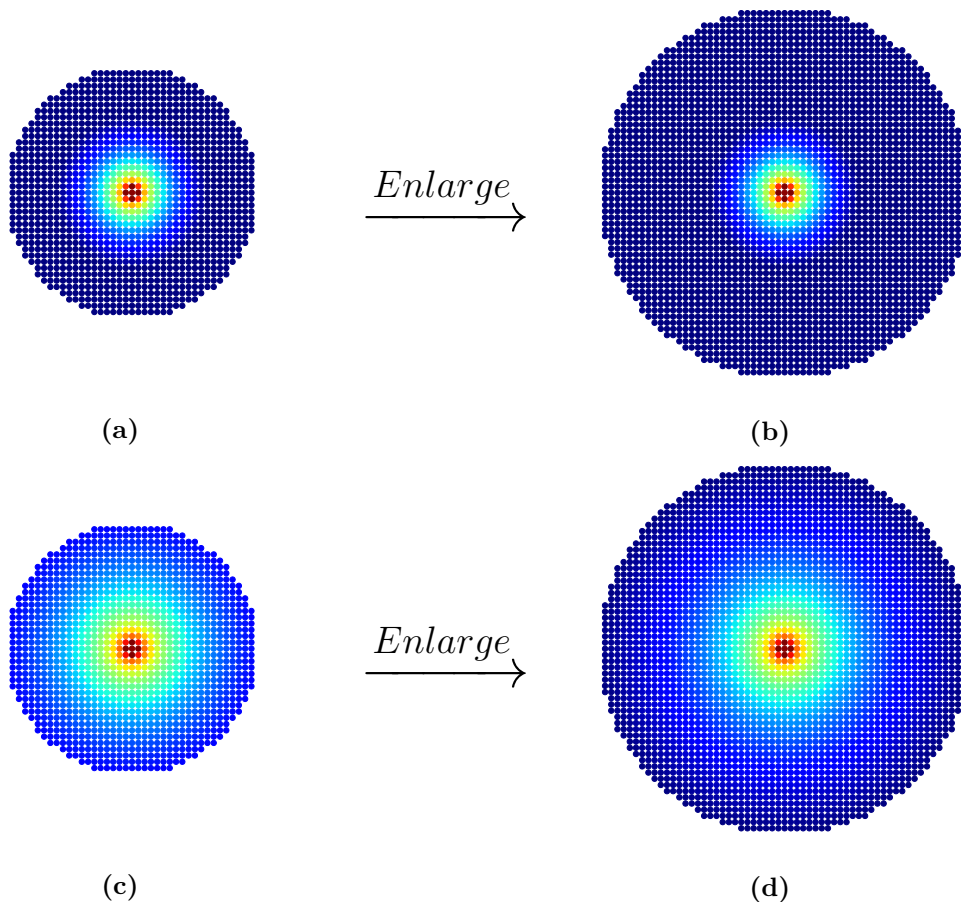


Figure 4: Illustrating final size effects by showing a fictional probability distribution of an excitation for $t \rightarrow \infty$ in a lattice. Whereas the system size in (a) is sufficiently large to detect localization, the extent of the expansion in (c) is too widespread. Increasing the system size isn't needed in case of a & b, but for c it is required.

If the mean displacement for $t \rightarrow \infty$ doesn't increase with the system size, the excitation is considered as localized!

Unfortunately there is a limit. At some certain point we won't be able to increase the system size further, due to restricted computing capacities. Therefore a localized excitation with a significantly large localization length can't be detected. The finite size effect prevails over a numerical proof for every localization length.

4 How to simulate spin transport

The simulation should provide an efficient time evolution of a single excitation placed in a gas of Rydberg atoms.

We start with generating a random configuration of N atoms in a two dimensional plane, while paying attention to the constraint of our Rydberg blockade radius r_b . The atoms are placed within a circle of radius \mathcal{R} being at least separated by r_b . An important system parameter is the scaled density ρ , which quantifies the packing density of Rydberg blockade spheres. It is calculated with $\rho = \frac{N\pi r_b^2}{\pi \mathcal{R}^2}$. Note, that one can't generate samples with arbitrarily high density. Although the densest packing density of circles in a two dimensional plain is the hexagonal arrangement with $\rho = 0.9069$, those high densities are not possible to achieve by random placements. By numerical testing we found out that the highest possible density, we can generate, lies around $\rho \sim 0.52$.

Additionally every atom receives a number for identification. The order of the numbers doesn't matter.

4.1 Hilbert space

The state of an single atom can either be the ground state $|\downarrow\rangle$ or the excited state $|\uparrow\rangle$. To describe the whole system for a specific moment in time a N -dimensional vector $|\uparrow\rangle_1 \otimes |\downarrow\rangle_2 \otimes \dots \otimes |\downarrow\rangle_N = |\uparrow\downarrow \dots \downarrow\rangle$ is needed. This state would describe a system in which the excitation sits on the site labeled by 1.

By knowing that we only have a single preserved excitation, it is possible to shorten this notation to $|i\rangle$, which means that the site with label i is excited and every other atom is in the ground state.

All possible states are contained in the Hilbertspace:

$$\begin{aligned} \mathcal{H} &= \{|\uparrow\downarrow \dots \downarrow\rangle, |\downarrow\uparrow \dots \downarrow\rangle, \dots, |\downarrow\downarrow \dots \uparrow\rangle\} \\ &= \{|100 \dots 0\rangle, |010 \dots 0\rangle, \dots, |000 \dots 1\rangle\} \\ &= \{|1\rangle, \quad |2\rangle, \dots, \quad |n\rangle\} \end{aligned} \tag{4.1}$$

4.2 Hamiltonian

In order to provide the spin dynamics, we use a spin Hamiltonian. This kind of Hamiltonian has (almost always) a sum of one-spin and two-spin terms comparable to a Hamiltonian (4.3) of a particle system, where one has one-body terms (external potential) and two-body terms (particle-particle interactions).

For investigating spin dynamics based on dipolar interaction, the dipolar XY spin Hamiltonian is suitable [3]:

$$H = \sum_{ij} V_{ij}(S_i^+ S_j^- + S_i^- S_j^+) + \sum_i E_i S_i^z \quad (4.2)$$

This kind of Hamiltonian describes a spin transfer between different sites i and j , where S^\pm are the spin raising and lowering operators, E_i are the on-site energies and V_{ij} is the matrix element of the dipole-dipole interaction.

It is possible to generalize this concept of spin transfer to a universal form of particle transport by rewriting this Hamiltonian [9].

$$H = \sum_i \sum_{j \neq i} t_{ij} c_i^\dagger c_j + \sum_i E_i c_i^\dagger c_i \quad (4.3)$$

The operator c_i^\dagger removes a particle from site i , E_i is again the on-site energy and t_{ij} is the amplitude for particle tunneling from site i to site j .

To keep the option open to go to higher numbers of excitations, we will stick to the XY spin Hamiltonian in (4.2), because in case of multiple excitations the mapping to the particle picture becomes more complicated.

4.2.1 Spin operators

S_k are the spin- $\frac{1}{2}$ angular momentum operators and arise through the Pauli matrices $S_k = \frac{1}{2}\sigma_k$ with $k = \{x, y, z\}$. Note, that $\hbar = 1$. In matrix notation:

$$S_x = \frac{1}{2} \begin{pmatrix} 0 & 1 \\ 1 & 0 \end{pmatrix} \quad S_y = \frac{1}{2} \begin{pmatrix} 0 & -i \\ i & 0 \end{pmatrix} \quad S_z = \frac{1}{2} \begin{pmatrix} 1 & 0 \\ 0 & -1 \end{pmatrix} \quad (4.4)$$

S^+ and S^- are the spin raising and lowering operators defined as $S^\pm = S_x \pm iS_y$.

$$S_+ = \begin{pmatrix} 0 & 1 \\ 0 & 0 \end{pmatrix} \quad S_- = \begin{pmatrix} 0 & 0 \\ 1 & 0 \end{pmatrix} \quad (4.5)$$

The properties of the spin raising and lowering operators are the following:

$$S^+ |\downarrow\rangle = \begin{pmatrix} 0 & 1 \\ 0 & 0 \end{pmatrix} \begin{pmatrix} 0 \\ 1 \end{pmatrix} = |\uparrow\rangle \quad S^+ |\uparrow\rangle = 0 \quad (4.6)$$

$$S^- |\uparrow\rangle = \begin{pmatrix} 0 & 0 \\ 1 & 0 \end{pmatrix} \begin{pmatrix} 1 \\ 0 \end{pmatrix} = |\downarrow\rangle \quad S^- |\downarrow\rangle = 0 \quad (4.7)$$

The operators S_i^\pm act on the atom with label i . The product of $S_i^+ S_j^-$, acting on an arbitrary state of the Hilbert space, describes a spin exchange. S_i^+ raises the spin on site i and S_j^- lowers the spin on site j .

$$S_i^+ S_j^- |\downarrow \dots \downarrow^i \dots \uparrow^j \dots \downarrow\rangle = |\downarrow \dots \uparrow^i \dots \downarrow^j \dots \downarrow\rangle \quad (4.8)$$

This means the excitation moves from site j to site i .

Due to the single excitation we actually don't need the other term $S_i^- S_j^+$. Nevertheless we leave it for the completeness.

In our notation a spin exchange can now be expressed by:

$$(S_i^+ S_j^- + S_i^- S_j^+) |i\rangle = |j\rangle \quad (4.9)$$

4.2.2 Hopping Hamiltonian

Working with a single excitation makes our life even easier, as we can simplify the XY spin Hamiltonian (4.2) to a standard hopping Hamiltonian:

$$H = \sum_{i=1}^N E_i |i\rangle \langle i| + \sum_{i \neq j}^N V_{ij} |i\rangle \langle j| \quad (4.10)$$

The hopping from site i to j is determined by the transition amplitude V_{ij} , while E_i are the on-site potentials:

$$H_{ij} = \langle i | H | j \rangle = \begin{cases} E_i, & i = j \\ V_{ij}, & i \neq j \end{cases} \quad (4.11)$$

As already said, we investigate spin dynamics based on the dipole-dipole interaction $V_{ij} = \frac{C}{|r_i - r_j|^3}$. Consequently we will work with the following Hamiltonian:

$$H = \sum_{i=1}^N E_i |i\rangle \langle i| + \sum_{i \neq j}^N \frac{C}{|r_i - r_j|^3} |i\rangle \langle j| \quad (4.12)$$

The coupling strength C determines the timescale of the transport and could be set to 1, which just rescales the time. Nevertheless we try to simulate the dynamics as realistic as possible. That's why we stick to SI-units and use $C/2\pi = 0.434 \text{ GHz } \mu\text{m}^3$ with reference to [3].

Additionally we will work without on-site energies, meaning $E_i = 0 \forall i$. Randomness of the on-site energies is probably the most common and easiest approach to numerically simulate Anderson localization. Usually a lattice is taken and impact of the randomness on the localization behavior is investigated. A number of studies using this partially filled lattice geometry exists [20, 19, 9]. In contrast, our ansatz is based on generating randomness only by the random placement of the atoms.

4.3 Time evolution

The time evolution is generated by the method of exact diagonalization. Once the Hamiltonian is built only a few steps remain.

The Hamiltonian generates the time evolution of quantum states. If $|\Psi(t)\rangle$ is the state of the system at time t , then the time evolution is described by the Schrödinger equation:

$$H |\Psi(t)\rangle = i\hbar \frac{\partial}{\partial t} |\Psi(t)\rangle \quad (4.13)$$

Given an initial state $|\Psi(t_0)\rangle$ (in our case $|i\rangle$), one can solve it to obtain the state at any subsequent time. If H is time independent, the time evolution can be written as

$$|\Psi(t)\rangle = e^{-i\frac{Ht}{\hbar}} |\Psi(t_0)\rangle \quad (4.14)$$

At ultra cold temperatures and for the evolution times typically considered, positions can be assumed as frozen. This leads to a time-independent Hamiltonian. Since H is just determined by the distances of the different atom pairs, one can write (4.12) as a time-independent matrix:

$$H = \begin{pmatrix} E_1 & V_{12} & V_{13} & & \\ V_{21} & E_2 & V_{23} & \dots & \\ V_{31} & V_{32} & E_3 & & \\ & \vdots & & \ddots & \end{pmatrix} \quad (4.15)$$

Exact diagonalization gives us the energy eigenvalues $\{\lambda_i\}$ and energy eigenvectors $\{E_i\}$. For the time evolution one starts by breaking the state $|i\rangle$ down in components of the eigenvectors by inserting unity $\mathbb{1}$:

$$|i\rangle = \sum_k |E_k\rangle \langle E_k|i\rangle \quad (4.16)$$

The time evolution of the state $|i\rangle$ results from the time evolution of the energy eigenstates:

$$\begin{aligned} |\Psi_i(t)\rangle &= \sum_k e^{-i\lambda_k t} |E_k\rangle \langle E_k|i\rangle \\ &= \sum_n |n\rangle \underbrace{\sum_k e^{-i\lambda_k t} \langle n|E_k\rangle \langle E_k|i\rangle}_{c_{in}(t)} \end{aligned} \quad (4.17)$$

In the second line another $\mathbb{1} = \sum_n |n\rangle \langle n|$ was inserted. Equation (4.17) describes the time evolution of a single excitation initially sitting on atom i .

4.3.1 Probability

For describing a transport behavior we are interested in knowing the population of all sites, i.e. the probability $P_{i \rightarrow j}(t) \forall j$. It describes, how likely it is to find the excitation after an arbitrary time t on atom j , with the initial condition that the excitation started out on atom i .

In general, the transition probability from one quantum state $|\psi_i\rangle$ to another $|\psi_j\rangle$ is defined as the absolute square $|\langle\psi_i|\psi_j\rangle|^2$. In our case, one needs to calculate the absolute square between the state of interest $|j\rangle$, i.e. where we wish to measure, and the time evolved initial state $|\Psi_i(t)\rangle$. The probability $P_{i \rightarrow j}(t)$ is given by:

$$\begin{aligned} P_{i \rightarrow j}(t) &= |\langle j|\Psi_i(t)\rangle|^2 = \left| \langle j| \sum_n |n\rangle \sum_k e^{-i\lambda_k t} \langle n|E_k\rangle \langle E_k|i\rangle \right|^2 \\ &= \left| \delta_{jn} \sum_k e^{-i\lambda_k t} \langle n|E_k\rangle \langle E_k|i\rangle \right|^2 \\ &= \left| \sum_k e^{-i\lambda_k t} \langle j|E_k\rangle \langle E_k|i\rangle \right|^2 \\ &= |c_{ij}(t)|^2 \end{aligned} \quad (4.18)$$

Infinite time average

Besides the spread of the excitation for finite times, it is quite interesting to know the probability distribution for $t \rightarrow \infty$. This can help, calculating properties of the transports (e.g. localization length) at infinite time or deciding whether the timeframe of the simulation is sufficiently large.

Therefor the probability $P_{i \rightarrow j}(t)$ from equation (4.18) can be partitioned further:

$$\begin{aligned} P_{i \rightarrow j}(t) &= |c_{ij}(t)|^2 = \left| \sum_k e^{-i\lambda_k t} \langle j|E_k\rangle \langle E_k|i\rangle \right|^2 \\ &= \left(\sum_k e^{-i\lambda_k t} \langle j|E_k\rangle \langle E_k|i\rangle \right) \cdot \left(\sum_{k'} e^{i\lambda_{k'} t} \langle i|E_{k'}\rangle \langle E_{k'}|j\rangle \right) \\ &= \sum_k |\langle j|E_k\rangle|^2 |\langle E_k|i\rangle|^2 + \sum_{k \neq k'} e^{-i(\lambda_k - \lambda_{k'})t} \langle j|E_k\rangle \langle E_k|i\rangle \langle i|E_{k'}\rangle \langle E_{k'}|j\rangle \end{aligned} \quad (4.19)$$

The asymptotic probability to start at site i and be at site j can be defined as [19]:

$$P_{i \rightarrow j}(t \rightarrow \infty) = \lim_{T \rightarrow \infty} \frac{1}{T} \int_0^T dt P_{i \rightarrow j}(t) \quad (4.20)$$

After inserting (4.19) into (4.20), the sum over $k \neq k'$ drops out (assuming no degeneracies), because it just describes a rotation in the complex plain, which cancels itself in the average.

We are left with:

$$P_{i \rightarrow j}(t \rightarrow \infty) = \sum_k |\langle j | E_k \rangle|^2 |\langle E_k | i \rangle|^2 \quad (4.21)$$

As we can see, the only factors determining the probability for $t \rightarrow \infty$ are the energy eigenstates of the Hamiltonian. Therefore exact diagonalization of the Hamiltonian is enough for calculating the probability distribution at infinite time.

4.4 Limitations

Implementing the time evolution was fairly straightforward, the challenge rather was the simulations efficiency, that was definitely needed. The first attempts took several minutes of computation time for just a few atoms (< 50), which was obviously not suitable simulating an atomic cloud with thousands of atoms.

With a continuous development of our code, we reached a point, where not the time evolution is the crucial factor, but the method of exact diagonalization. As it turned out the diagonalization of the Hamiltonian, which is for 10000 atoms a (10000×10000) -matrix, is not feasible. Regardless however, we decided to continue employing this technique, as we additionally wanted to investigate eigenstate properties. Consequently the limitation of simulating transport in a system of 10000 atoms was accepted.

4.5 Disorder averaging

The quantum transport of only one excitation traveling through a particular arrangement of atoms is highly affected by the individual positions leading to fluctuations. The results can be improved by averaging. Two different methods are possible for this process.

Firstly we can generate different configurations of arrangements of the atoms, where the initial excitation is always placed in the center of the plain. As a result the transport is a radial expansion.

Secondly it is possible to average over different time evolutions using the same configuration, but placing the initial excitation on a different atom in the beginning. So the time evolution is calculated for spreads starting from different atoms while diffusing through the same arrangements of atoms. Here attention has to be paid, that one doesn't average over completely different atoms, which don't obey the same diffusion process. The atoms should be relatively close ensuring that one receives comparable transport behaviors.

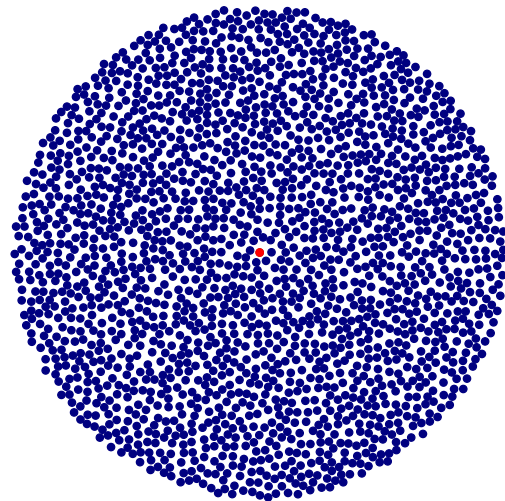


Figure 5: Random configuration. We always place the initial excitation in the middle of a circle with radius \mathcal{R} and density ρ

To avoid wrong averages we use the first method and generate different arrangements of atoms, where we place the initial excitation on the atom in the middle. Then the uniform radial propagations from the center of the plane are averaged.

5 Transport properties

Now that notation and the theoretical ansatz was presented, it is time to introduce physical quantities, which we will use to characterize the transport. We avail ourselves of:

- Mean square displacement $\langle r^2(t) \rangle$
- Mean displacement $\langle r(t) \rangle$
- Standard deviation $\sigma(t)$
- Distribution width $\mathcal{L}(t)$
- Participation ratio $\Pi_{|\Psi\rangle}$
- radial density $\rho(r)$

In the following those properties are specified. Note that $\langle r^2(t) \rangle$, $\langle r(t) \rangle$, $\sigma(t)$ and $\mathcal{L}(t)$ should have more or less the same meaning. However, we present all of them to underline the diffusion process.

5.1 Mean square displacement

The ability of diffusing through an ensemble can be measured by the mean square displacement (MSD) $\langle r^2(t) \rangle$ or respectively $\langle r(t) \rangle$. It is the most common measure of the spatial extent of random motion and characterizes the mean expansion. Before taking a closer look at our specific case, we want to give a brief review about transport types being relevant for the classification of our expansion.

5.1.1 Diffusive processes

It can be shown that the scaling behavior of $\langle r^2(t) \rangle$ depends on the type of transport. In general the transport process is characterized by a strictly monotonically increasing mean square displacement, while the growth is described by a power law in time [21]:

$$\langle r^2(t) \rangle \propto t^\alpha \tag{5.1}$$

One differentiates the following types:

- $0 < \alpha < 1$: subdiffusion
- $\alpha = 1$: normal diffusion
- $1 < \alpha < 2$: superdiffusion
- $\alpha = 2$: ballistic transport

Ballistic transport is defined as transport, where the scattering length (mean free path length) of the particles is large compared to the transport distance [22]. This means that a particle moves in a straight line from A to point B. Looking on a length scale much larger than the scattering length, there will be many scattering events, which interrupt the ballistic movement and slow it down [22]. The particle movement resembles now a random walk, instead of a straight line. This kind of process is called diffusion.

5.1.2 Mean square displacement of a quantum particle

Considering the excitation initially sitting on atom i , the mean displacement is the sum of distances between all atoms and atom i weighted with the probability $P_{i \rightarrow j}(t)$ of finding the excitation on the respective atom j . Therefore the mean displacement of the spread of an excitation starting on atom i is given by:

$$\langle r_i(t) \rangle = \sum_{j=1}^N |\langle j | \exp(-iHt) | i \rangle|^2 \cdot r_{ij} = \sum_{j=1}^N |\langle j | \Psi_i(t) \rangle|^2 \cdot r_{ij} = \sum_{j=1}^N P_{i \rightarrow j}(t) \cdot r_{ij} \quad (5.2)$$

$$\langle r_i^2(t) \rangle = \sum_{j=1}^N P_{i \rightarrow j}(t) \cdot r_{ij}^2 \quad (5.3)$$

With the probability distribution for $t \rightarrow \infty$ calculated in eq. (4.21), we can compute the MSD in the infinite time limit similarly by $\sum_{j=1}^N P_{i \rightarrow j}(t \rightarrow \infty) \cdot r_{ij}^2$.

The MSD is bounded above due to the finite size of our system. Its maximal value $\langle r^2 \rangle_{max}$ is obtained for a particle diffusing through an ideal lattice, since this would cause a perfectly uniform probability distribution for $t \rightarrow \infty$. In this case, we not only observe the diffusion, but also the reflection of the excitation from the edges [11]. Because of the constant radial distribution of the atoms, $\langle r^2 \rangle_{max}$ depends only on the system size \mathcal{R} and is given by:

$$\langle r \rangle_{max} = \frac{1}{\pi \mathcal{R}^2} \int_0^{\mathcal{R}} r \, dx dy = \frac{2}{3} \mathcal{R} \quad (5.4)$$

$$\langle r^2 \rangle_{max} = \frac{1}{\pi \mathcal{R}^2} \int_0^{\mathcal{R}} r^2 \, dx dy = \frac{1}{2} \mathcal{R}^2 \quad (5.5)$$

5.2 Distribution width

We define the distribution width as the radius of the circle containing 90% of the excitation probability. Using 90% has no deeper significance, this value was chosen arbitrarily. \mathcal{L} helps characterizing the physical spread of the excitation over the ensemble of atoms [20].

5.3 Standard deviation

Another important quantity representing the physical spread is the standard deviation determining the amount of variation. It depends on the shape of the probability distribution and should be less affected by fluctuations than the distribution width.

In our case the standard deviation σ can be computed by:

$$\begin{aligned}
\sigma_i^2(t) &= \sum_j^N (r_{ij} - \langle r_i(t) \rangle)^2 \cdot P_{i \rightarrow j}(t) = \sum_j^N (r_{ij}^2 - 2r_{ij} \langle r_i(t) \rangle + \langle r_i(t) \rangle^2) \cdot P_{i \rightarrow j}(t) \\
&= \sum_j^N r_{ij}^2 \cdot P_{i \rightarrow j}(t) - \sum_j^N 2r_{ij} \langle r_i(t) \rangle \cdot P_{i \rightarrow j}(t) + \sum_j^N \langle r_i(t) \rangle^2 \cdot P_{i \rightarrow j}(t) \\
&= \langle r_i^2(t) \rangle - 2\langle r_i(t) \rangle^2 + \langle r_i(t) \rangle^2 \\
&= \langle r_i^2(t) \rangle - \langle r_i(t) \rangle^2
\end{aligned} \tag{5.6}$$

Note, that $\sigma_i^2(t) \approx \langle r_i^2(t) \rangle$, if the mean position does not move, which we would assume for a homogeneous system.

Localization length

The standard deviation is well qualified quantizing localization due to its connection to the localization length. The localization length ξ is defined by the exponential decay of the wavefunction:

$$\Psi(x) \propto \exp\left(-\frac{|x - x_0|}{\xi}\right) \tag{5.7}$$

Starting with a wavefunction $\Psi(x) = A \exp\left(-\frac{|x - x_0|}{\xi}\right)$, A is fixed to $A = \xi^{-\frac{1}{2}}$ by the condition for the probability normalization:

$$P = \int_{-\infty}^{\infty} |\Psi(x)|^2 dx \stackrel{!}{=} 1 \tag{5.8}$$

The standard deviation is given by:

$$\begin{aligned}
\Delta x &= \sqrt{\langle \Psi | x^2 | \Psi \rangle - \langle \Psi | x | \Psi \rangle^2} \\
(\Delta x)^2 &= \frac{1}{\xi} \int_{-\infty}^{\infty} x^2 e^{-\frac{2|x-x_0|}{\xi}} dx - \underbrace{\left(\frac{1}{\xi} \int_{-\infty}^{\infty} x e^{-\frac{|x-x_0|}{\xi}} dx \right)^2}_{=0} \\
&= \frac{\xi^2}{2}
\end{aligned} \tag{5.9}$$

The second integral equals 0 because of integrating an antisymmetric function over a symmetric interval.

We obtain a relation between the localization length and the standard deviation:

$$\xi = \sqrt{2} \cdot \Delta x \tag{5.10}$$

The standard deviation is therefore an ideal quantity to describe Anderson localization. Note, that this is just the case when dealing with exponentially decaying wavefunctions.

5.4 Participation ratio

The inverse participation ratio (IPR) represents over how many states a particle/excitation is distributed. It measures the spread of a state $|\Psi\rangle$ over a basis $\{|i\rangle\}_{i=1}^N$ or space. More precisely, if $P_j = |\tau_j|^2$ is the probability of finding the state $|\Psi\rangle = \sum_i \tau_i |i\rangle$ in $|j\rangle$, then the IPR is defined as:

$$I_{|\Psi\rangle} = \sum_j |\tau_j|^4 \quad (5.11)$$

However, for descriptive reasons we work with the participation ratio (PR), which is defined as the inverse of the IPR:

$$\Pi_{|\Psi\rangle} = I_{|\Psi\rangle}^{-1} = \frac{1}{\sum_j |\tau_j|^4} \quad (5.12)$$

In 1D the PR is directly proportional to the localization length [23].

In a system of size N , a fully delocalized state $|\Psi\rangle = \sum_j \frac{1}{\sqrt{N}} |j\rangle$, which is evenly divided over N states with probability $P_i = \frac{1}{N} \forall |i\rangle$, corresponds to

$$\Pi_{|\Psi\rangle} = \frac{1}{\sum_j^N |\frac{1}{\sqrt{N}}|^4} = \frac{1}{N \cdot \frac{1}{N^2}} = N \quad (5.13)$$

If a particle/excitation is localized and covers only a single site, then $P_j = 1$ for some state $|j\rangle$, so $\Pi_{|\Psi\rangle} = 1$.

As demonstrated, the participation ratio can just occupy values between 1 and N and can therefore be used as a measure for localization.

In our case the PR is calculated for arbitrary time t to determine the time dependence of the participating states:

$$\Pi_{|\Psi_i(t)\rangle} = \frac{1}{\sum_j^N |\langle j|\Psi_i(t)\rangle|^4} = \frac{1}{\sum_j^N P_{i \rightarrow j}^2(t)} \quad (5.14)$$

Infinite time average

Additionally we are again interested in computing the PR for $t \rightarrow \infty$. Therefore we firstly calculate the time average for the IPR and subsequently use the definition of the participation ratio, being the inverse of the IPR:

$$I_{|\Psi_i(t \rightarrow \infty)\rangle} = \lim_{T \rightarrow \infty} \frac{1}{T} \int_0^T I_{|\Psi_i(t)\rangle} dt = \lim_{T \rightarrow \infty} \frac{1}{T} \int_0^T \left(\sum_j^N |\langle j|\Psi_i(t)\rangle|^4 \right) dt \quad (5.15)$$

$$\Pi_{|\Psi_i(t \rightarrow \infty)\rangle} = I_{|\Psi_i(t \rightarrow \infty)\rangle}^{-1} = \frac{1}{\lim_{T \rightarrow \infty} \frac{1}{T} \int_0^T \left(\sum_j^N |\langle j|\Psi_i(t)\rangle|^4 \right) dt} \quad (5.16)$$

Reminding ourselves of previous calculations for $|\langle j|\Psi_i(t)\rangle|^2$ in equation (4.19):

$$\begin{aligned}
|\langle j|\Psi_i(t)\rangle|^2 &= P_{i\rightarrow j}(t) \\
&= \sum_k |\langle j|E_k\rangle|^2 |\langle E_k|i\rangle|^2 + \sum_{k\neq k'} e^{-i(\lambda_k-\lambda_{k'})t} \langle j|E_k\rangle \langle E_k|i\rangle \langle i|E_{k'}\rangle \langle E_{k'}|j\rangle \\
&= P_{i\rightarrow j}(t \rightarrow \infty) + \sum_{k\neq k'} e^{-i(\lambda_k-\lambda_{k'})t} \langle j|E_k\rangle \langle E_k|i\rangle \langle i|E_{k'}\rangle \langle E_{k'}|j\rangle
\end{aligned} \tag{5.17}$$

Now to compute equation (5.15) we need to square equation (5.17) and single out the real components, since only they are contributing in the time average.

Additional real parts arise from the second term with the sum:

$$\begin{aligned}
\mathbf{Re}(|\langle j|\Psi_i(t)\rangle|^4) &= (P_{i\rightarrow j}(t \rightarrow \infty))^2 + \mathbf{Re}\left[\left(\sum_{k\neq k'} e^{-i(\lambda_k-\lambda_{k'})t} \langle j|E_k\rangle \langle E_k|i\rangle \langle i|E_{k'}\rangle \langle E_{k'}|j\rangle\right)^2\right] \\
&= (P_{i\rightarrow j}(t \rightarrow \infty))^2 + \mathbf{Re}\left[\sum_{k\neq k'} e^{-i(\lambda_k-\lambda_{k'})t} \langle j|E_k\rangle \langle E_k|i\rangle \langle i|E_{k'}\rangle \langle E_{k'}|j\rangle\right. \\
&\quad \left.\times \sum_{z\neq z'} e^{-i(\lambda_z-\lambda_{z'})t} \langle j|E_z\rangle \langle E_z|i\rangle \langle i|E_{z'}\rangle \langle E_{z'}|j\rangle\right]
\end{aligned} \tag{5.18}$$

The complex phase in the sum drops out for $k = z'$ and $k' = z$.

$$\begin{aligned}
\mathbf{Re}(|\langle j|\Psi_i(t)\rangle|^4) &= (P_{i\rightarrow j}(t \rightarrow \infty))^2 \\
&\quad + \sum_{k\neq k'} \langle j|E_k\rangle \langle E_k|i\rangle \langle i|E_{k'}\rangle \langle E_{k'}|j\rangle \langle j|E_{k'}\rangle \langle E_{k'}|i\rangle \langle i|E_k\rangle \langle E_k|j\rangle \\
&= (P_{i\rightarrow j}(t \rightarrow \infty))^2 + \sum_{k\neq k'} |\langle j|E_k\rangle|^2 |\langle E_k|i\rangle|^2 |\langle i|E_{k'}\rangle|^2 |\langle E_{k'}|j\rangle|^2 \\
&= \dots
\end{aligned} \tag{5.19}$$

We make use of separating the sum $\sum_{k\neq k'} = \sum_k \cdot \sum_{k'} - \sum_{k=k'}$, so that we can trace some terms back to our known $P_{i\rightarrow j}(t \rightarrow \infty)$:

$$\begin{aligned}
\dots &= (P_{i\rightarrow j}(t \rightarrow \infty))^2 + \sum_k |\langle j|E_k\rangle|^2 |\langle E_k|i\rangle|^2 \cdot \overbrace{\sum_{k'} |\langle i|E_{k'}\rangle|^2 |\langle E_{k'}|j\rangle|^2}^{P_{i\rightarrow j}(t \rightarrow \infty)} \\
&\quad - \sum_{k=k'} |\langle j|E_k\rangle|^2 |\langle E_k|i\rangle|^2 |\langle i|E_{k'}\rangle|^2 |\langle E_{k'}|j\rangle|^2 \\
&= (P_{i\rightarrow j}(t \rightarrow \infty))^2 + (P_{i\rightarrow j}(t \rightarrow \infty))^2 - \sum_k |\langle j|E_k\rangle|^4 |\langle E_k|i\rangle|^4 \\
&= 2 \cdot (P_{i\rightarrow j}(t \rightarrow \infty))^2 - \sum_k |\langle j|E_k\rangle|^4 |\langle E_k|i\rangle|^4
\end{aligned} \tag{5.20}$$

Concluding, the participation ratio for $t \rightarrow \infty$ is given by:

$$\Pi_{|\Psi_i(t \rightarrow \infty)\rangle} = \left[\lim_{T \rightarrow \infty} \frac{1}{T} \int_0^T \left(\sum_j^N |\langle j | \Psi_i(t) \rangle|^4 \right) dt \right]^{-1} \quad (5.21)$$

$$= \left[\sum_{j=1}^N \left(2 \cdot (P_{i \rightarrow j}(t \rightarrow \infty))^2 - \sum_k |\langle j | E_k \rangle|^4 |\langle E_k | i \rangle|^4 \right) \right]^{-1} \quad (5.22)$$

5.5 Accumulated probability and radial density

To measure how the probability decreases radially, we firstly calculate the probability of finding the excitation further away from its center x_0 than distance r :

$$n(r, t) = \sum_{j: |x_j - x_0| \in [r, \mathcal{R}]} P_{i \rightarrow j}(t) \quad (5.23)$$

Therefore we always obtain $n(0, t) = 1$, since we sum over the whole 2D plane and $n(\mathcal{R}, t) = 0$. We will use $n(r, t)$ mainly for illustration purposes, since it features nicely the difference of localized and non localized states.

Secondly, the radial density is computed by summing up the probabilities in equal annuli and dividing by the number of atoms within this area.

$$\rho(r, t) = \sum_{j: |x_j - x_0| \in [r, r + \Delta]} \frac{1}{K} P_{i \rightarrow j}(t) \quad (5.24)$$

K is the number of atoms for which $|x_j - x_0| \in [r, r + \Delta]$ is true.

We set the thickness of the rings Δ to $2r_b$.

Having defined now all relevant physical quantities, as well as knowing their calculation, we are ready to investigate the spin dynamics.

6 Microscopic mechanism

In order to understand how spin transport based on a hopping Hamiltonian works, we start with a small number of atoms, where the dynamics are illustrated nicely. Therefore we manually designed some scenarios, which are meaningful and can help us understand the expansion in a much bigger system.

In our considered context, we are working without on-site energies. As a consequence the Hamiltonian and its dynamics only depend on the distances between the placed atoms. Intuitively one would expect that atoms situated closer to the initial excitation would be more susceptible to excitation. In the following we want to show how far this is accurate and which exceptions may occur.

We illustrate the path, which the excitation travels by presenting the time evolution of the probability meeting the excitation at the different atoms (figures on the right side).

The simplest case is built with 2 atoms. Here the probability to find the excitation at one of the atoms is periodically oscillating. This is the same as Rabi-oscillations in a two-level system.

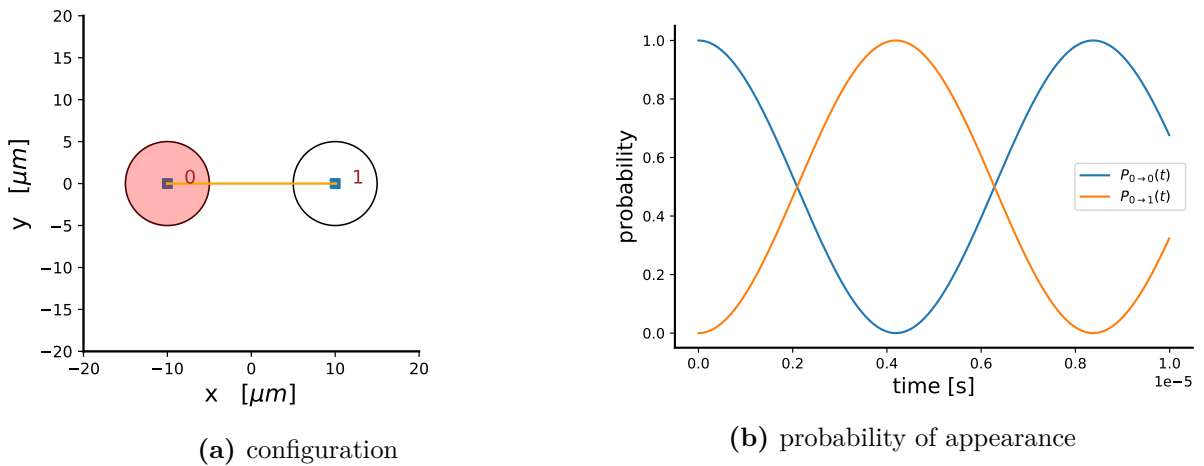


Figure 6: Illustrating spin dynamics with 2 atoms. Initially the excitation was placed on atom labeled with 0. (a) shows the arrangements of the atoms and (b) presents the probability finding the excitation at one of the atoms.

By expanding the system to larger ensembles, a greater variety of dynamics is noticeable. One of it is the formation of a dressed state shown in figure 7a and 7b with 8 atoms.

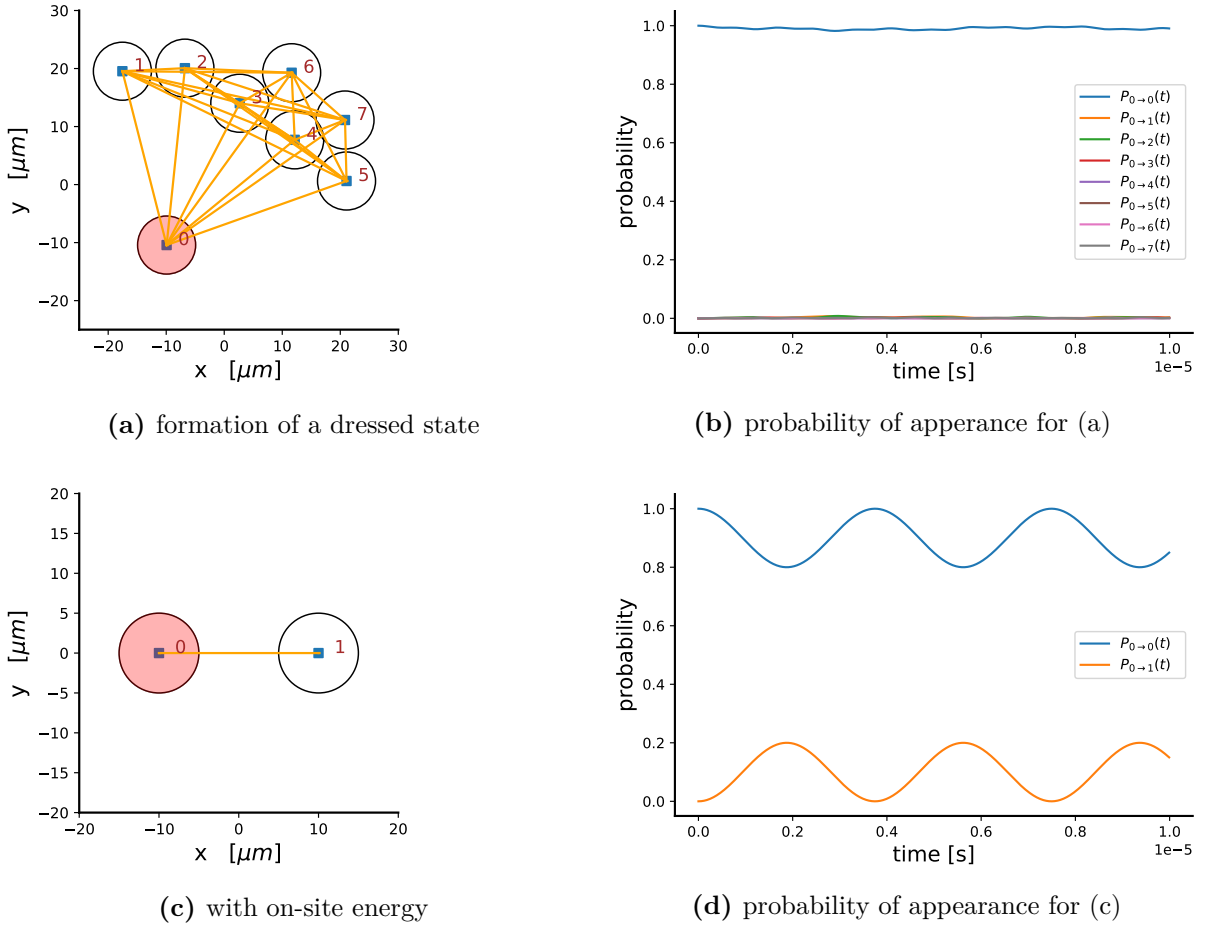


Figure 7: Time evolution of an excitation transfer in an ensemble with 8 atoms. Initially the excitation was placed on atom labeled with 0. In (c) the case of (a) is reproduced by placing on-site energies on the atoms. Note that (c) and (d) should only qualitatively illustrate the reduction of the complexity. We didn't calculate the dressed states for (a). Increasing the on-site energies would suppress the dynamics.

6.1 Dressed states

Let us now aim to explain the behavior illustrated in figures 7a and 7b. We notice how the atoms with index $i > 0$ form a cluster, which wards off the excitation coming from atom 0. This cluster forms a dressed state.

Our Hamiltonian consists of an atomic part (diagonal) and an interaction part (off-diagonal). A dressed state is defined as an eigenstate of the total Hamiltonian or a subblock of the total Hamiltonian, i.e an eigenstate of both the atomic and interaction part [24]. Once these dressed states are found, and their energies known, the dynamics of the system is simple: the total state is a superposition of these states [24].

Knowing the dressed states, it is possible to understand the suppressed dynamics of figure 7a and 7b and to reproduce it by using 2 atoms.

For simplicity we explain this procedure by starting with 3 atoms, and not 8. The Hamiltonian is given by:

$$H = \begin{pmatrix} 0 & V_{01} & V_{02} \\ V_{10} & 0 & V_{12} \\ V_{20} & V_{21} & 0 \end{pmatrix} \quad (6.1)$$

In case of figure 8, atoms 1 and 2 are forming a cluster due to their small distance. For the dressed states, we diagonalize the sub-block of the Hamiltonian which includes those 2 atoms. We obtain the eigenstates:

$$|+\rangle = \frac{1}{\sqrt{2}} [|1\rangle + |2\rangle] \quad (6.2)$$

$$|-\rangle = \frac{1}{\sqrt{2}} [|1\rangle - |2\rangle] \quad (6.3)$$

Corresponding eigenvalues are $+V_{12}$ and $-V_{12}$.

The resulting dressed states $|+\rangle$ and $|-\rangle$ couple now to the remaining state $|0\rangle$. This coupling can be calculated by:

$$\Delta_+ = \langle 0 | H | + \rangle = \frac{1}{\sqrt{2}} [V_{01} + V_{02}] \quad (6.4)$$

$$\Delta_- = \langle 0 | H | - \rangle = \frac{1}{\sqrt{2}} [V_{01} - V_{02}] \quad (6.5)$$

In the end one obtains a detuning and a coupling for every dressed state. Rewriting the Hamiltonian (6.1) in the basis $|0\rangle, |+\rangle, |-\rangle$ yields:

$$H = \begin{pmatrix} 0 & V_{01} & V_{02} \\ V_{10} & 0 & V_{12} \\ V_{20} & V_{21} & 0 \end{pmatrix} \rightarrow \begin{pmatrix} 0 & \Delta_+ & \Delta_- \\ \Delta_+ & +V_{12} & 0 \\ \Delta_- & 0 & -V_{12} \end{pmatrix} \quad (6.6)$$

The dynamics of the upper left (2×2) -sub-block of (6.6) would be strongly suppressed in the case of $V_{01}, V_{02} \ll V_{12}$. This is shown in figures 7c and 7d by using 2 atoms and placing on one atom a on-site energy. It corresponds to the case of detuning for a two level system, i.e. the frequency of the laser is slightly off from a quantum system's resonant frequency.

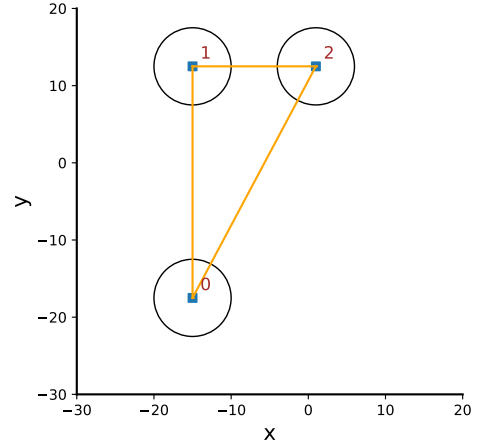


Figure 8: Atom 1 and 2 are close together, whereas atom 0 is situated remotely. Atom 1 and 2 form a cluster, which can cause a detuning, leading to suppressed dynamics

6.2 Short distances

Due to the fact that our dynamics is only distance depended, two atoms located relatively close to each other, compared to surrounding atoms, will mainly interact among each other. While ignoring the other atoms, the excitation will oscillate between those near atoms. Additionally one would expect, that the transport speed scales inversely with the distance of the positional separation, meaning the exchange is enhanced the closer the atoms are [5]. This effect can be seen in figure 9a and 9b, where the initial excitation was placed on atom labeled with 1, being close to atom 2. The probability of finding the excitation oscillates quickly between those two near atoms, while being almost zero for every other atom.

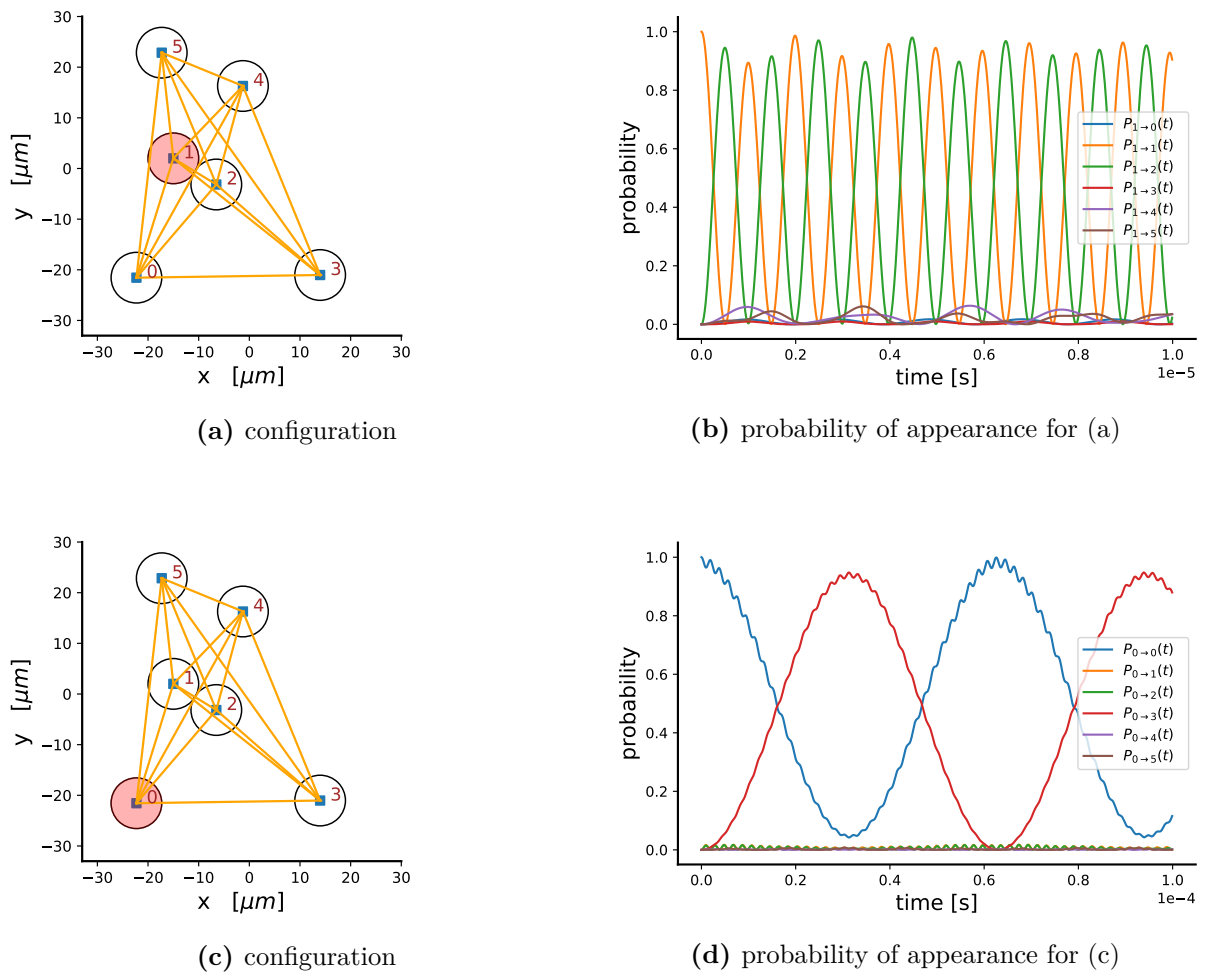


Figure 9: Illustrating the behavior of a system with two or more atoms situated closely. Whereas in (a) and (b) the excitation is placed on one of the atoms of the pair, in (c) and (d) another atom is excited.

On the other hand two or more atoms, which are situated closely, won't be easily excited. This is illustrated in figure 9c and 9d, which show the same configuration, albeit with the initial excitation placed on atom 0. Although the pair of atoms (1 and 2) is closer to the initial excitation than any other atom, the excitation rather jumps to atom 3.

In conclusion, atoms with small distances will speed up the short range transport, but suppress the long range transport. This is because an excitation sitting initially at one of these atoms will be confined, as can be seen in figure 9a and 9b.

Overall using those small manually designed scenarios, spin transport could be understood for certain configurations and it was possible to comprehend, why some atoms are excited and others remain untouched.

However, generally there is no way to know exactly where the full dynamics arises from. An example is given in figure 10, where we used the configuration of figure 9 and just changed the position of atom 4 and 5 slightly.

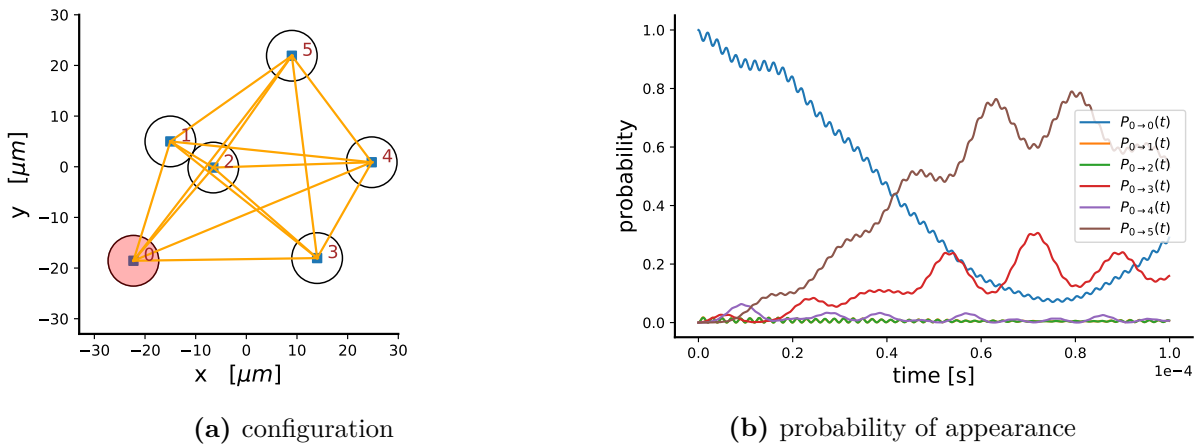


Figure 10: Illustrating the complexity of spin dynamics. Same configuration was used as in figure 9, only with slightly differences in the arrangement. We receive dynamics, which differs a lot from the dynamics shown in figure 9d.

Changing the positions slightly can lead to major changes in the microscopic dynamics. Even so, the dynamics at a global scale is rather robust to such changes, see following chapters.

Using this knowledge of small-scale spin dynamics, we are more able to understand transport behavior in a larger extent. This will be investigated in the next chapter.

7 Numerical results: Transport behavior

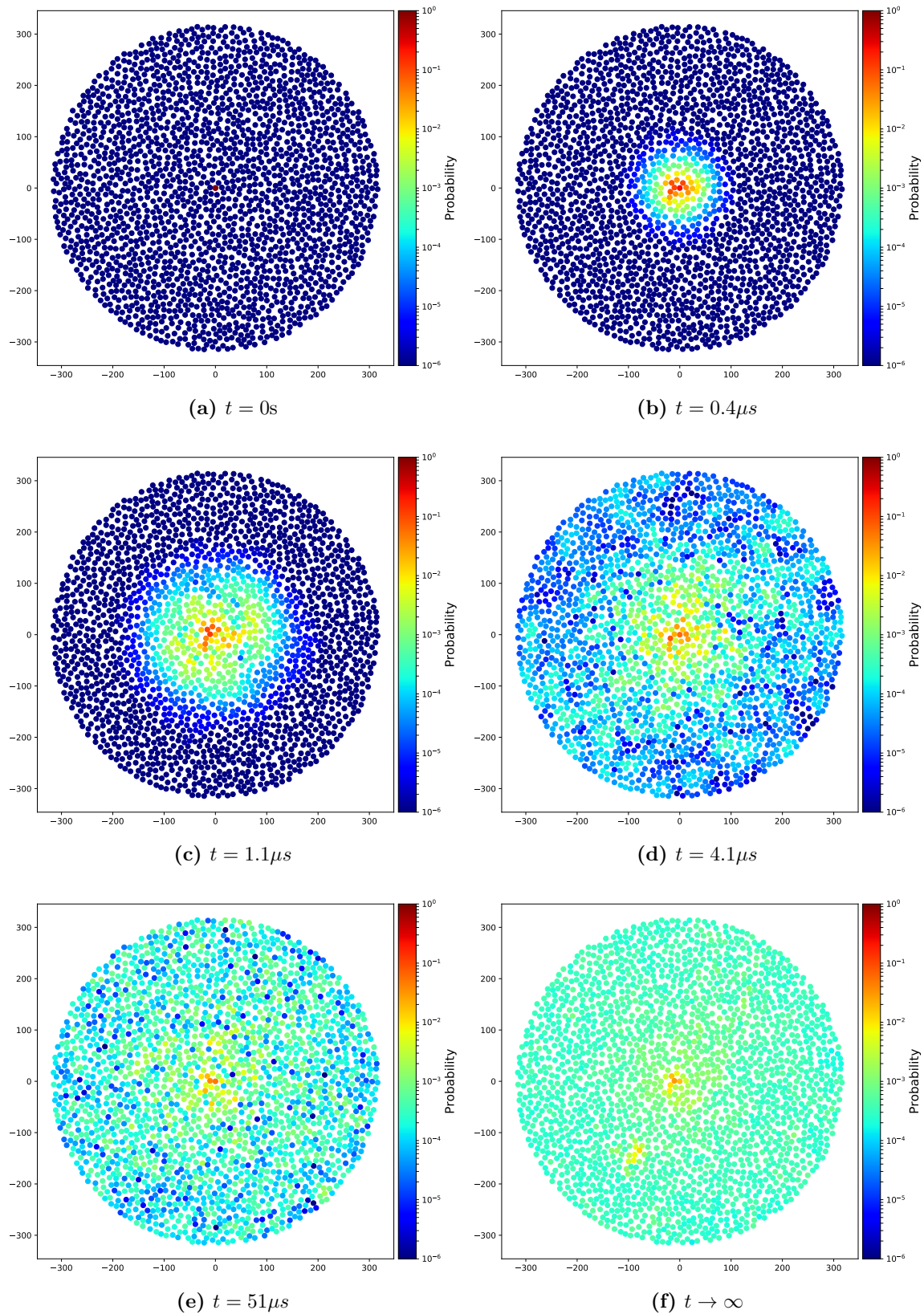


Figure 11: Example for an expansion of a single excitation in a system of 2000 atoms at a density of $\rho = 0.5$ and a Rydberg blockade radius of $r_b = 10\mu m$. System size is $\mathcal{R} \approx 316\mu m$. The probability of meeting the excitation was calculated for different times and is shown in colors.

Figure 11 shows an example for the expansion of a single spin excitation. As one can see the excitation starts spreading evenly in all directions. This process can be illustrated by the time dependence of the accumulated probability $n(r, t)$ (figure 12), which represents the probability of finding the excitation further away than distance r . For increasing times (different colors) $n(r, t)$ increases as well, meaning the excitation spreads. For $t \rightarrow \infty$ the probability decreases steadily, but one has $n(r, t \rightarrow \infty) > 0$ even for large r . This indicates that the excitation is not localized or that the system size is too small to see the localization.

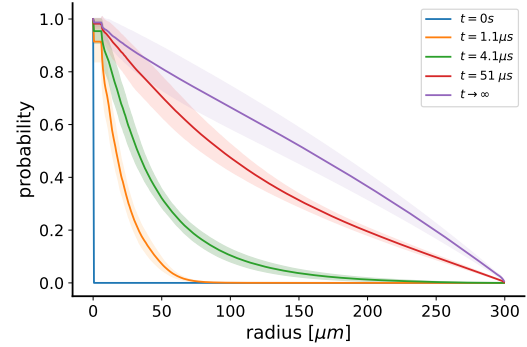


Figure 12: Probability of finding the excitation further away than radius r is shown for different times. "Radius" on the x-axis means that our distances are always with reference to the center of the plane.

7.1 Mean square displacement

For the classification of the kind of transport process, we computed the MSD for different times as well as for infinity. Figure 13 shows $\langle r^2(t) \rangle$ for our standard case $r_b = 10 \mu m$, and compares the spread of our excitation with two additional Rydberg blockade radii, namely $r_b = 6$ and $2 \mu m$.

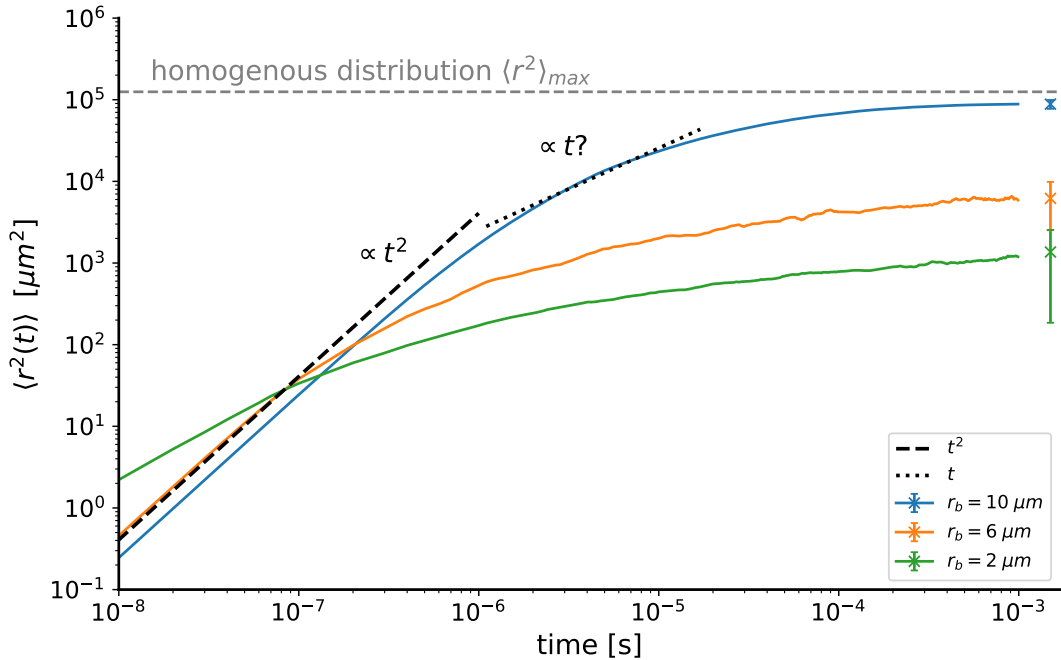


Figure 13: Time dependence of the mean square displacement $\langle r^2(t) \rangle$ simulated with a system of 5000 atoms in random arrangements for different Rydberg blockade radius $r_b = 10, 6, 2 \mu m$ at fixed system size of $\mathcal{R} = 500 \mu m$ each averaged over 200 configurations. The colored area shows the standard deviation of those averages. The markers on the right side represent $\langle r^2(t) \rangle$ for $t \rightarrow \infty$. Note that the plot is in log log scale.

Regardless of the Rydberg blockade radius the excitation starts spreading quickly, then slows down until it stagnates.

We start examining the curve for $r_b = 10\mu m$. In an attempt to explain the evolution of our MSD, we considered first the three standard cases: ballistic, diffusive and subdiffusive. However, after some considerations we arrived at the conclusion, that we are dealing with a steady transition between an initial ballistic dynamics, combined with a saturation-like end. In order to verify this kind of transport behavior, we attempted to fit power laws to the MSD shown in figure 13. Our results confirmed the prior conclusion, that the initial spread is driven by ballistic behavior, i.e. we observe a projectile like evolution $\langle r^2(t) \rangle \propto t^2$.

For intermediate times there is no well-marked segment for a diffusive or subdiffusive propagation. The curve seems more like a smooth decline of the gradient.

At the end the MSD almost equals $\langle r^2 \rangle_{max}$, resulting in a homogeneous distribution.

Compared to the other blockade radii, the MSD is "extremal" for $r_b = 10\mu m$, i.e the lowest initially and largest at late times. Conversely for $r_b = 2$ the MSD is highest for small times and lowest for large times. This is exactly what we expect, referring back to our toy models with <10 atoms. We estimated that, bringing the atoms closer together would speed up the short range transport, but suppress the long range transport. Due to the confined excitations caused by closely situated atoms, the spread is not able to generate a homogeneous distribution.

Saturation

An interesting question which arises is, why a saturation effect seems to develop. Why does the expansion of the excitation slow down after a ballistic start and even comes to rest in the large time limit?

The saturation is either caused by the reflection from the boundaries of the system, or by Anderson localization. Obviously the first case occurs when the spread of the excitation reaches the limits of the system due to finite size effect. Of more interest and complexity is the second scenario, where the propagation stagnates after some time due to interferences. Although the excitation has enough space to propagate, the transport slows down and saturates.

In the following section we investigate, whether the departure of the MSD from a ballistic propagation $\langle r^2(t) \rangle \propto t^2$ is due to localization or finite size effects. Once this is done, we want to clarify the impacts by which the localization behavior can be influenced.

8 Numerical results: Anderson Localization

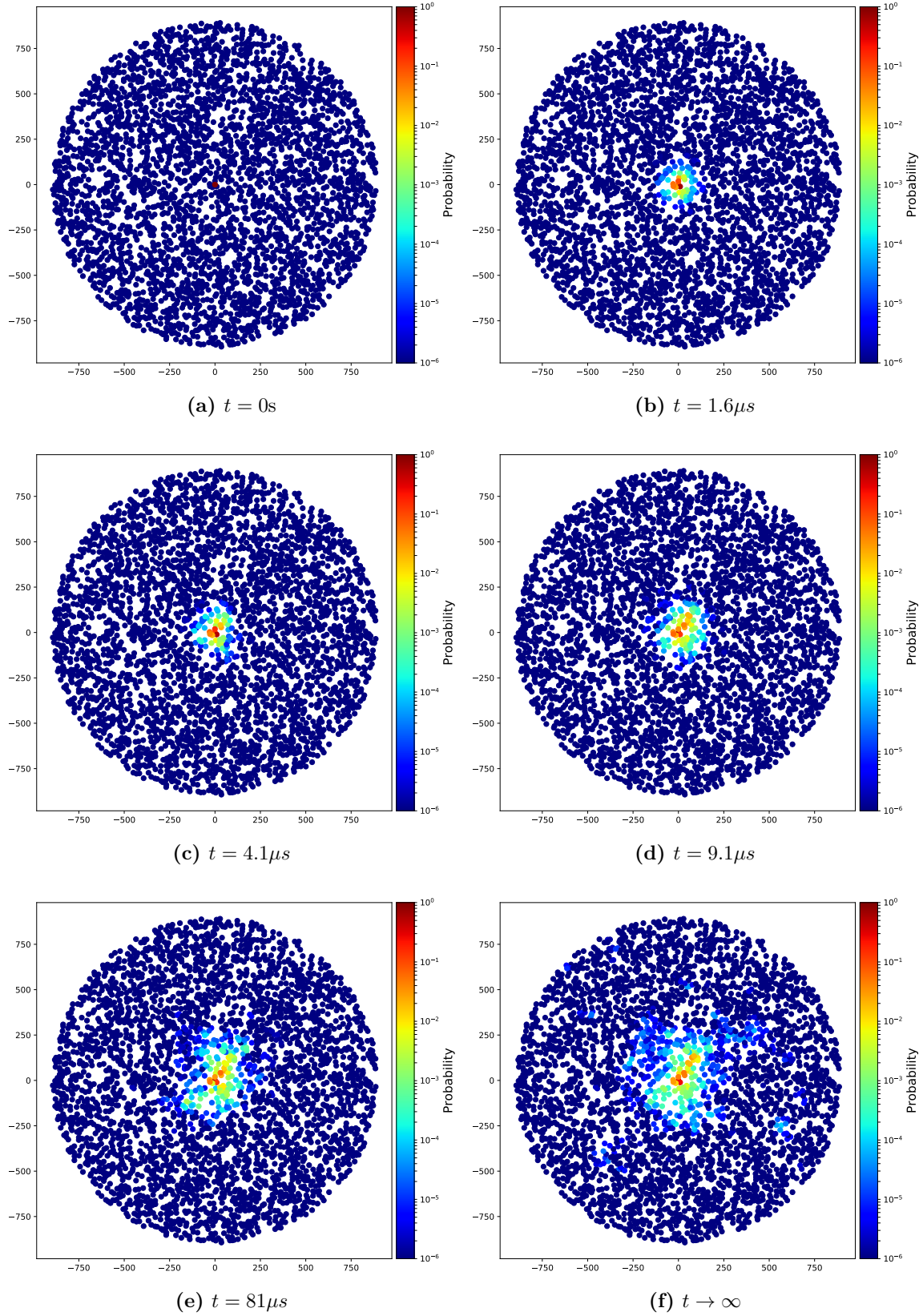


Figure 14: Illustrating localization effects. The expansion of a single excitation in a system of 3200 atoms at a density of $\rho = 0.1$ with a Rydberg blockade radius of $r_b = 10\mu\text{m}$ is shown. System size is $\mathcal{R} = 900\mu\text{m}$.

Figure 14 shows an example expansion involving localization behavior. As opposed to figure 11, a completely different state is obtained for $t \rightarrow \infty$, due to changing the density from $\rho = 0.5$ to $\rho = 0.1$. The quantitative difference to the expansion without localization can be seen in figure 15. While $n(r, t \rightarrow \infty)$ in case of non localization decreases steadily with the radius (fig. 12), here $n(r, t \rightarrow \infty)$ decreases faster. The excitation seems to be confined in a much smaller area than the system size.

The probability to meet the excitation further away than $400\mu m$ remains almost zero, even for infinite t . As a whole, the excitation seems to be trapped, with a probability dropping fast from the center of the plane.

In the following we are going to present two totally different transport scenarios, one affected by localization and one not. The focus in the next section is showing the differences between transport properties for both processes.

8.1 Localization and density

This section aims at clarifying the difference between a localized and delocalized excitation. We want to motivate qualitatively the influence of the density (\sim randomness) on our localization behavior. We then turn to our quantitative study of the explicit density dependence.

The excitation transfer was computed at two different densities: $\rho = 0.5$ and 0.1 . As was already mentioned, we try to distinguish saturation due to localization or finite size effect by varying the system size. All quantities, which are going to be presented should be independent of the system size, if the excitation is localized!

For both densities we calculated the expansion for three different system sizes:

For $\rho = 0.5$:

- 3200 atoms with $\mathcal{R} = 400\mu m$
- 5000 atoms with $\mathcal{R} = 500\mu m$
- 7200 atoms with $\mathcal{R} = 600\mu m$

For $\rho = 0.1$:

- 3200 atoms with $\mathcal{R} \approx 894\mu m$
- 5000 atoms with $\mathcal{R} \approx 1118\mu m$
- 7200 atoms with $\mathcal{R} \approx 1342\mu m$

We averaged over 200 different disorder realizations.

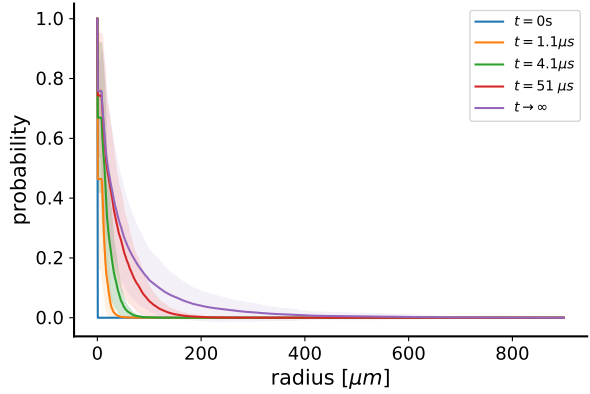


Figure 15: Probability of finding the excitation further away than radius r is shown for different times.

8.1.1 Meeting the excitation at the edge

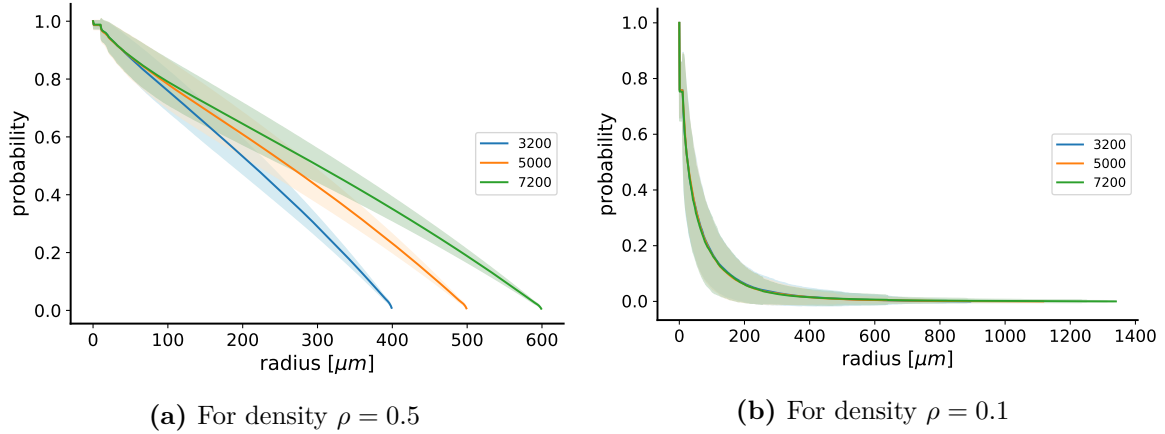


Figure 16: Probability of finding the excitation further away than distance r . Calculated for 3 different system sizes at constant density $\rho = 0.5$ and 0.1 . Again the colored area represents the standard deviation occurring through the averages.

In figure 16 the accumulated probability $n(r, t \rightarrow \infty)$ is presented once more, allowing a direct comparison. In 16a it can be seen, that the three different expansions differ a lot, while the decay in 16b seems to be equal regardless of the system size. Additionally for $\rho = 0.5$ one receives a probability $\neq 0$ to find the particle far outside, while it's almost zero for $\rho = 0.1$.

We conclude that for $\rho = 0.5$ no localization effect can be seen, caused by finite size effects. In contrast, for $\rho = 0.1$ we obtain true localization, since the three probability curves are equal.

8.1.2 Distribution width

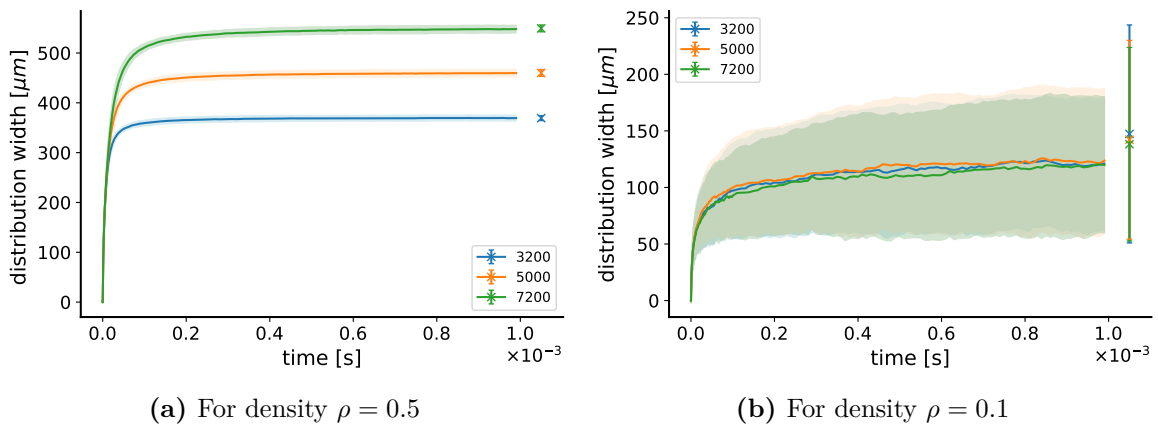


Figure 17: Time dependence of the distribution width (radius of a circle containing 90% of the excitation probability) for three different system sizes at fixed densities of $\rho = 0.5$ and $\rho = 0.1$

The distribution width (figure 17) characterizes the extent of the physical spread. For $\rho = 0.5$ the saturation ends at around $0.9\mathcal{R}$ for each system size \mathcal{R} , i.e. the expansion

has reached the boundaries. This differs quite a lot to $\rho = 0.1$, where the distribution width seems to be the same for the three cases. This indicates that the excitation is trapped in a circle with a radius of roughly \mathcal{L} . Comparing the finite distribution length \mathcal{L} it strikes, that $\mathcal{L}_{\rho=0.1}$ is a lot less than $\mathcal{L}_{\rho=0.5}$ as well as its boundaries. This means that the excitation in 17a can travel until reaching the boundaries, whereas the propagation in 17b stagnates already after $100\mu\text{m}$.

Additionally we note a high variance at low density. This is caused by the increased randomness of the arrangement of the atoms. The potentially bigger differences in the placements lead to higher fluctuations in our results.

8.1.3 Participation ratio

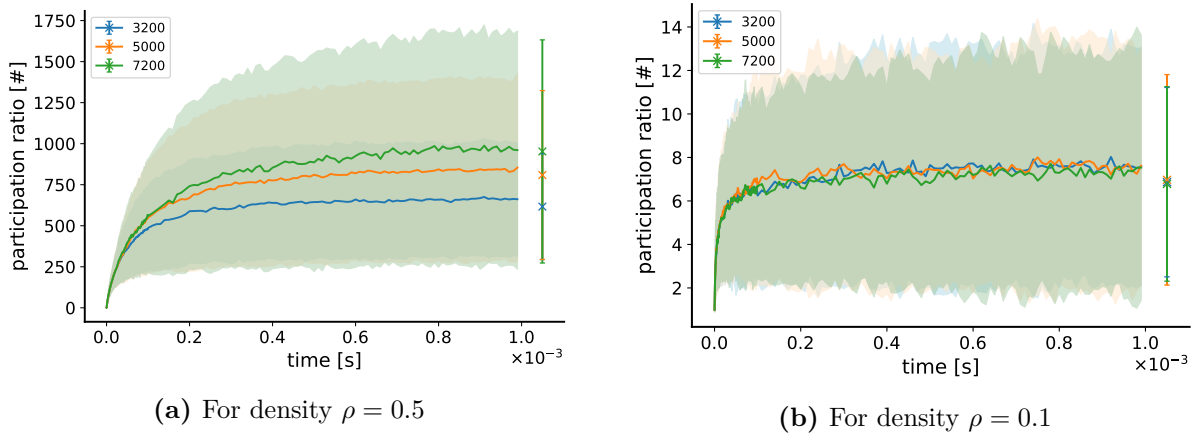


Figure 18: Time dependence of the participation ratio for three different system sizes at fixed densities of $\rho = 0.5$ and $\rho = 0.1$

The participation ratio represents the number of states over which the excitation is distributed, and therefore can indicate the extent of its expansion. In contrast to the high participation ratio in figure 18a, $\Pi_{\rho=0.1}$ saturates already at around 7 states. This suggests a highly localized final probability distribution and also explains the low distribution width in figure 17b. Consequently the excitation travels just a little and is subsequently confined.

Another feature we can observe is, that the PR suffers a lot from the high standard deviation, even for a high density $\rho = 0.5$. The variation of up to 1000 participating states demonstrate, how different a transport in a random ensemble can be, although using the same density.

8.1.4 MSD and MD

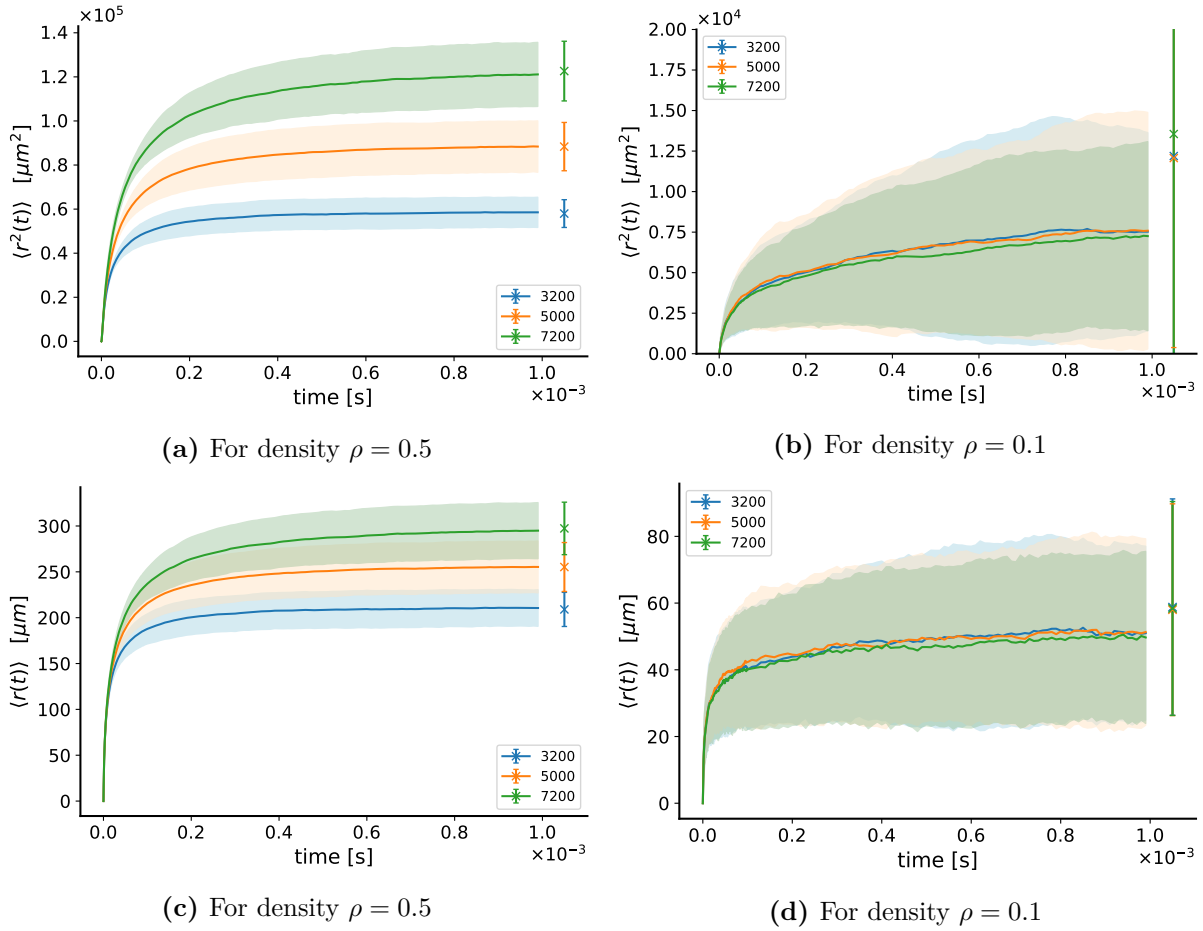


Figure 19: Time dependence of the mean square displacement and mean displacement computed for three different system sizes at two fixed densities $\rho = 0.5$ and $\rho = 0.1$.

The mentioned facts are supported by the curve of $\langle r^2(t) \rangle$ and $\langle r(t) \rangle$, since a similar scaling becomes apparent. The expansion is stopped by the boundaries for $\rho = 0.5$, due to the fact that $\langle r^2(t \rightarrow \infty) \rangle$ or $\langle r(t \rightarrow \infty) \rangle$ differ for different system sizes. In contrast, for $\rho = 0.1$ the MSD and MD is independent of system size, i.e. we see localization.

What is striking is that at low density (19b and 19d), the saturation isn't completely finished for the time scale considered. This is indicated by the values for infinite time, since they are a bit above our values for the last calculated time at $t = 10^{-3}$ s. A further expansion after $t = 10^{-3}$ s is also recognizable looking at the distribution width in figure 17b, but not supported by the curve of the PR in 18b. Here it seems that the participating states don't increase. This is not necessarily a contradiction, because the excitation can spread itself further without taking new atoms into account.

Nevertheless we can be sure that even for larger times the boundaries won't be reached, because the markers for $t \rightarrow \infty$ are far below $\langle r^2 \rangle_{max} = \frac{1}{2} \mathcal{R}^2$ and $\langle r \rangle_{max} = \frac{2}{3} \mathcal{R}$. As well as the evolution of the spread, the values for infinite time don't differ from each other, suggesting Anderson localization at low density.

Referring to the introduction Anderson localization requires $\langle r(t) \rangle < C$ uniformly in time. We could not only show a stagnated MD in figure 19d, but we also proved that we can exclude boundary effects due to system independence of our three measurement series. Therefore we can claim to see Anderson localization for a density of $\rho = 0.1$.

8.1.5 Localization length

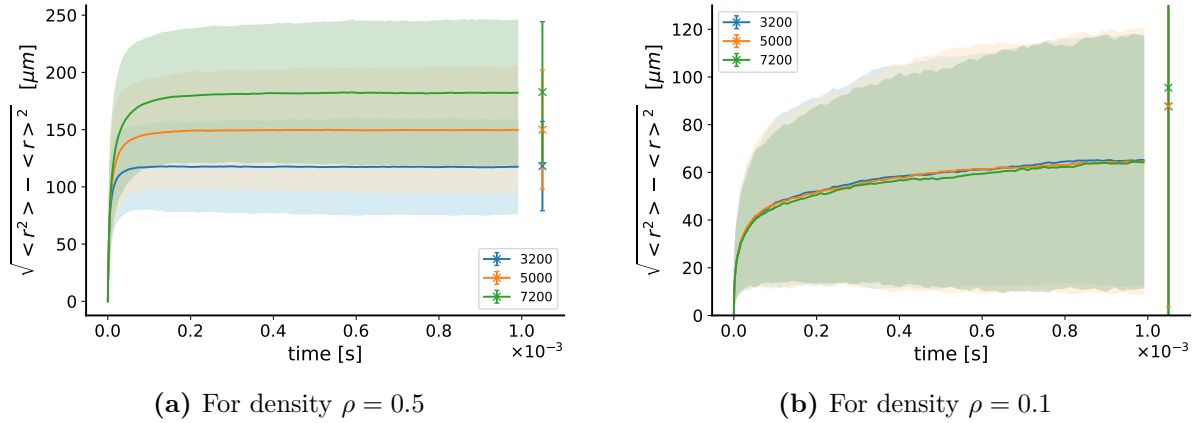


Figure 20: Time dependence of standard deviation of the mean displacement computed for three different system sizes at two fixed densities $\rho = 0.5$ and $\rho = 0.1$.

We considered two possible ways of determining the localization length. On the one hand, as we deduced the connection between the localization length and standard deviation in chapter 5 with $\xi = \sqrt{2} \cdot \sigma$, we thought it is justified to identify the curve of σ with the localization length. On the other hand, our second approach was to use the definition of the exponential decay

$$\propto \exp\left(-\frac{|x - x_0|}{\xi}\right) \quad (8.1)$$

and receive the localization length ξ through a fit to the radial density .

Both methods require an exponential decay of the wave function.

Unfortunately we were neither able to find such an exponential scaling nor an appropriate fit, meaning that both methods were not justified after all. Figure 21 shows for the two cases $\rho = 0.5$ and $\rho = 0.1$ the respective radial density.

Since we have already proved localization in case of $\rho = 0.1$, one would surmise exponential scaling. However this is not the case, as can be seen in figure 21b.

For $\rho = 0.5$ we observe a decrease given by $\propto t^{-1}$. Note the double logarithmic scale in 21a. In 21b only the y-axis is plotted logarithmically, for verifying an exponential decay, but even with good will an exponential fit would not be appropriate.

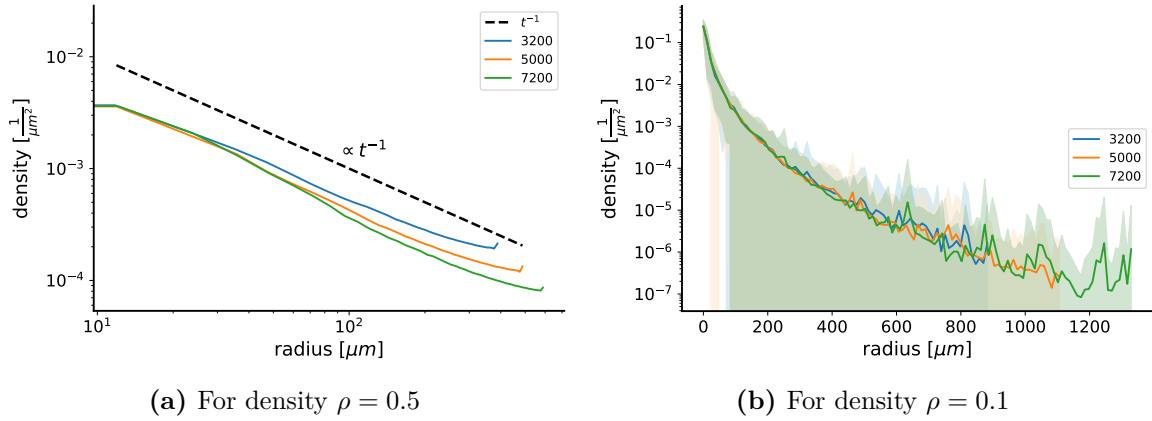


Figure 21: Illustrating the decay of the radial density computed for three different system sizes at two fixed densities $\rho = 0.5$ and $\rho = 0.1$.

In similar researches [20] they investigated Anderson localization of rotational excitations in disordered ensembles of polar molecules. As we did, they used the standard deviation as measure for the extent of the excitation. In 1D an exponential decay of the probability was found, but not in case of 2D and 3D. Additionally there wasn't a quantitative dependence between the localization length and the density presented. One could assume that the missing of the exponential decay is a quite common problem.

However, also other reasons might exist for the missing of an exponential decay. Perhaps Anderson localization does not enter purely in the way we assumed, but rather a more complex behavior and dynamics could be present. In this case it would be interesting to see, how slight modifications to Anderson localization could imprint themselves on the scaling and other properties. Regardless of the reason, this is an issue which needs further study and research.

A promising idea seems to be the approach of a stretched exponential decay $\propto \exp\left(-\left[\frac{r}{\xi}\right]^\alpha\right)$ [19].

Unfortunately we didn't succeed in establishing a quantitative connection between the density and the localization length. Nevertheless we still want to clarify the impact of the density (\sim randomness). As we were unable to verify our theoretical model providing the link between our density and the localization length, we proceed in the next section by empirical means. Through considering a varying density, we observe the change in expansion.

8.2 Density dependency

In the following we won't pay attention to the time dependent expansion anymore, but will investigate the dependence of the transport properties for $t \rightarrow \infty$ on the systems density. Therefore we computed the same quantities as before, but only for infinite time at the steady state, and compare them to each other for different densities.

As before we use for one density multiple system sizes to be able to distinguish finite size effects from localization. In case of localization, meaning low densities, we would expect quite similar results, since the transport and the final distribution has to be independent of the system size. But for high densities, where a observation of localization is not necessarily given due to finite size effects, we expect a behavior which scales with system size. Table 1 shows, which densities and respective sizes we used.

Density ρ	0,005	0,01	0,025	0,05	0,1	0,15	0,2	0,25	0,3	0,35	0,4	0,45	0,5
$\mathcal{R} : 700\mu m$													
Atoms	98	196	490	980	1960	2940	3920	4900	5880	6860	7840	8820	9800
# Avg	50000	30000	20000	6000	5000	2000	1000	500	300	150	70	50	30
$\mathcal{R} : 600\mu m$													
Atoms	72	144	360	720	1440	2160	2880	3600	4320	5040	5760	6480	7200
# Avg	50000	30000	20000	7000	2000	800	500	200	100	100	100	70	24
$\mathcal{R} : 500\mu m$													
Atoms	50	100	250	500	1000	1500	2000	2500	3000	3500	4000	4500	5000
# Avg	50000	40000	30000	15000	7000	3000	1500	1000	800	600	400	250	120
$\mathcal{R} : 400\mu m$													
Atoms	32	64	160	320	640	960	1280	1600	1920	2240	2560	2880	3200
# Avg	50000	40000	30000	20000	10000	5000	2000	1000	800	600	400	300	200

Table 1: We investigated 13 densities from $\rho = 0.005$ to 0.5 . For each density, four systems with different sizes and adjusted number of atoms are used to differentiate boundary effects from localization. The number of disorder averages for each configuration is shown as well. The Rydberg blockade radius is unchanged $r_b = 10\mu m$.

8.2.1 Participation ratio

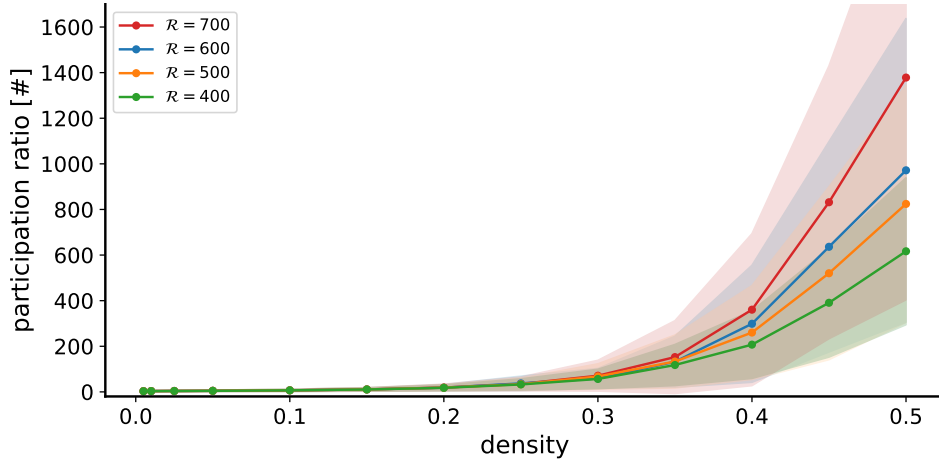


Figure 22: Density dependence of the participation ratio in the infinite time limit, computed for four different system sizes.

Figure 22 shows the participation ratio which increases for rising density, i.e. the final distribution of the excitation covers more and more atoms. Up to a density of approximately $\rho \sim 0.2$, it seems, that there is no difference of the PR for the four different sizes. Consequently we can assume localization for $\rho \leq 0.2$.

8.2.2 Distribution width

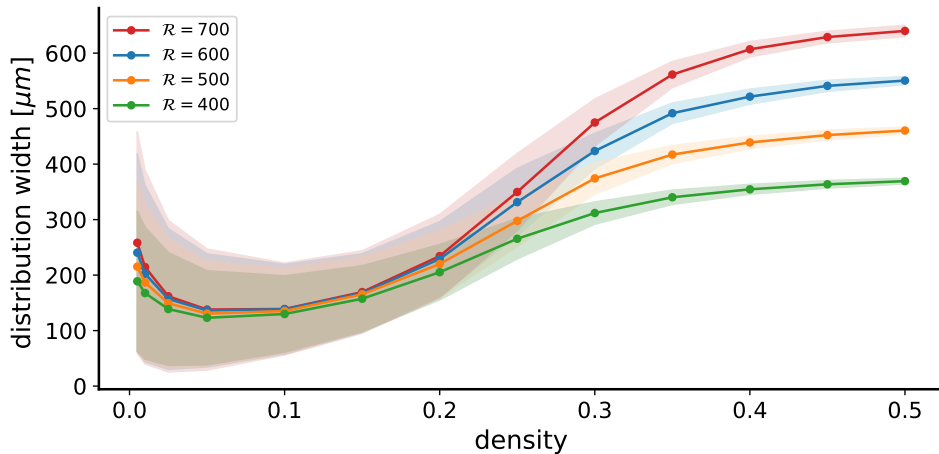


Figure 23: Density dependence of the distribution width in the infinite time limit, computed for four different system sizes.

As well as the PR, the distribution width doesn't differ in system size until $\rho \sim 0.2$. What attracts attention is the initial decrease between $\rho = 0$ and $\rho = 0.05$. Actually one would expect a positive monotonous gradient for the distribution width, similar to the evolution of the PR, since the extent of the excitation should increase until it reaches the

boundaries. The initial decrease does not only appear for the distribution width, but also is present in the following plots for $\langle r^2(t) \rangle$, $\langle r(t) \rangle$ and the standard deviation.

In order to understand this effect, we consider the following argument. From a certain density onwards ($\rho \leq \sim 0.05$) the Rydberg radius has no impact anymore. The positions are completely random, as the mean distance to the nearest neighbor is much larger than the blockade radius. Consequently the ratio of the distances among the atoms is unchanged for different densities, see figure 24. As a result, we can rescale our system, provided $\rho \leq 0.05$. Because the Hamiltonians differ from each other now only by a global factor, the eigenstates remain the same. As demonstrated in eq. (4.21), the probability distribution $P_{i \rightarrow j}(t \rightarrow \infty)$ depends only on the eigenstates. Now due to the unchanged eigenstates for different densities $\rho \leq 0.05$, we obtain again unchanged populations in the infinite time limit.

In the end, lowering the density increases quantities like $\langle r_i \rangle = \sum_{j=1}^N P_{i \rightarrow j} \cdot r_{ij}$, because the distances r_{ij} enlarge and the population remains the same.

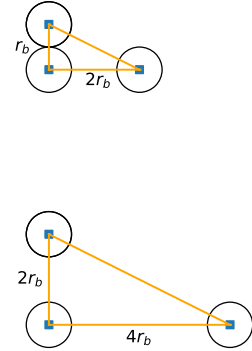


Figure 24: The lower configuration can be rescaled to the upper one by the factor 2.

8.2.3 MSD and MD

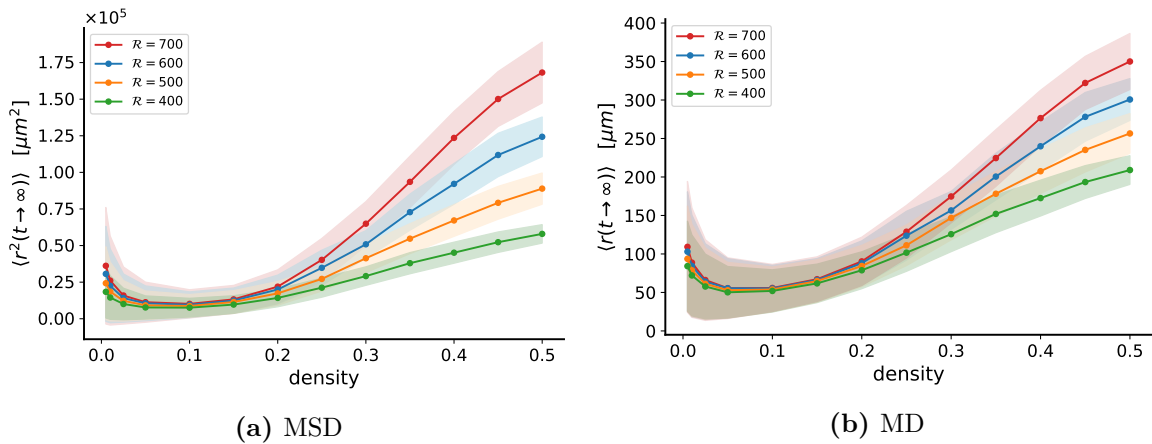


Figure 25: Density dependence of the mean square displacement and the mean displacement in the infinite time limit, computed for four different system sizes

As well as before, we observe localization for $\rho < 0.2$, due to fact that the curves of the MSD and MD are equal for the different system sizes.

However, since the MSD represents the ability of diffusing through an ensemble, one can draw conclusions about the suitability of different densities for transport.

As it can be seen in figure 25, the MSD remains low for small densities, i.e. the long range transport is suppressed. This proves that for a fast and far reaching transport, one requires maximally dense lattices. Nevertheless, it should not be forgotten that in such dense systems also localization phenomena arise. Only because we were unable to show localization effects at densities higher than $\rho \sim 0.2$, it does not mean that such effects do not occur at all. Rather, the localization length becomes comparable, and even larger than the system size, such that finite size effects prevent their detection.

One could easily observe localization at higher densities by increasing the system size a fifth or a sixth time. But that's exactly the curse of proving Anderson localization numerically. At a certain point your computing capacities are exhausted and you are not able to increase the number of atoms and the respective system size further. Unfortunately we reached this limit with our measurement series (red), using a system size of $\mathcal{R} = 700\mu\text{m}$ and 9800 atoms.

8.2.4 Standard deviation

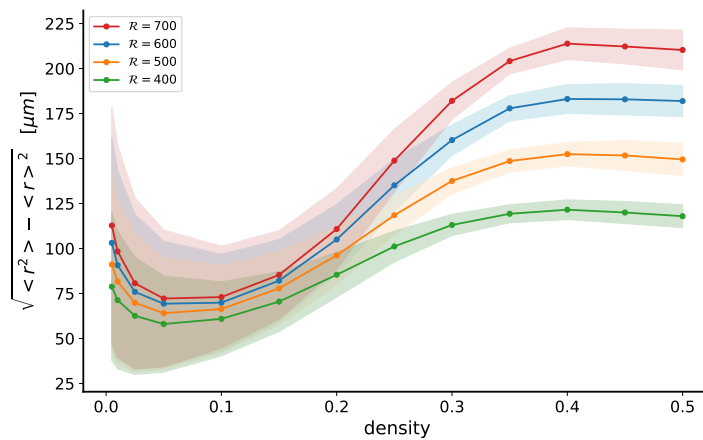


Figure 26: Density dependence of the standard deviation in the infinite time limit, computed for four different system sizes

At this point we hoped to present the standard deviation shown in figure 26 as a final result, equating it with the localization length, such that a dependency between density and localization length would be provided. But as already mentioned we cannot identify the standard deviation with the localization length as initially imagined, due to the non exponential decrease of our radial density.

Although the approach of exact diagonalization restricts the number of atoms we can simulate, in the next chapter the method pays off, since it enables to investigate individual energy eigenstates and their statistical properties.

9 Energy eigenstates

The eigenstate properties can be totally different in different parts of the spectrum, as can be seen in figure 27. Here the population of an eigenstate is plotted for the ground state, as well as the highest energy eigenstate for a system with 5000 atoms and $\rho = 0.5$.

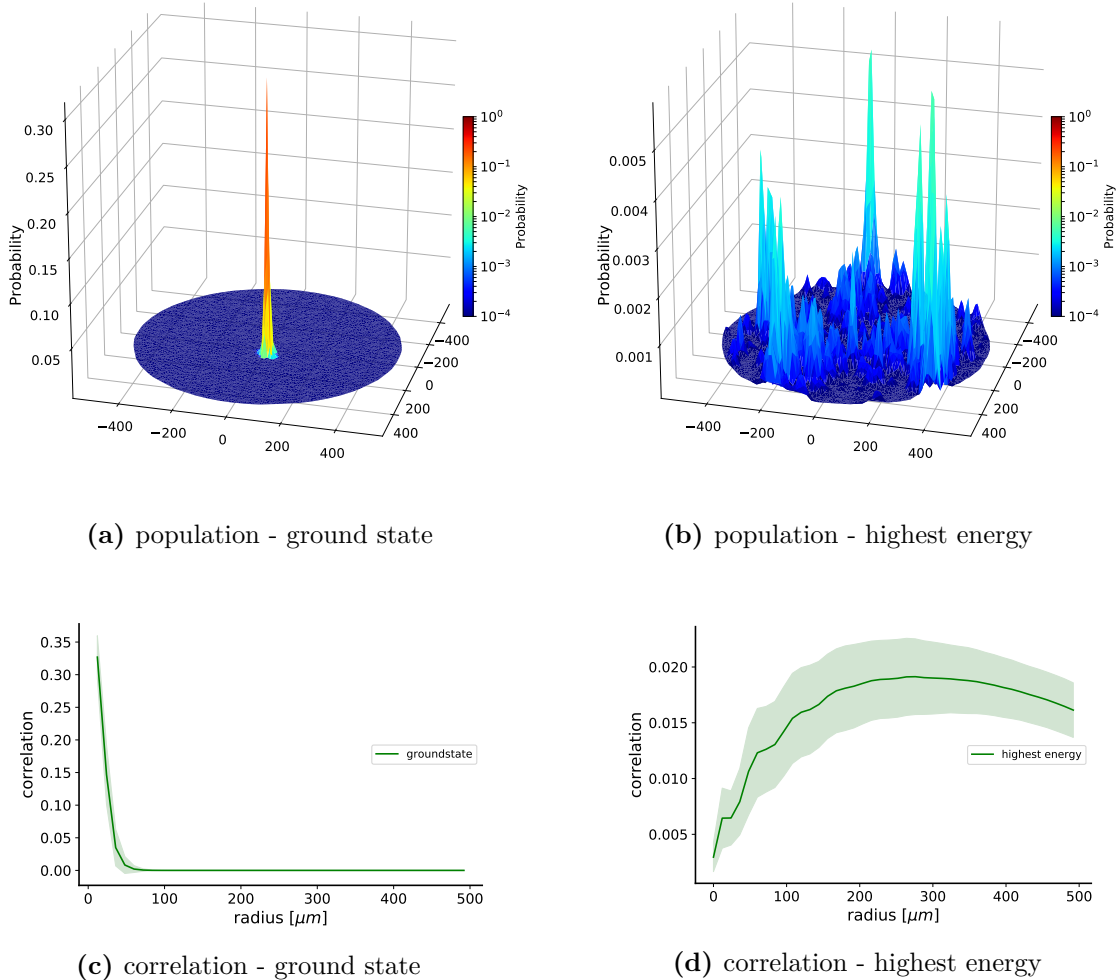


Figure 27: Distributions of the population and the correlation functions for the groundstate and state with the highest eigenvalue. For the correlation functions we averaged over 200 ground states or the state with the highest energy and used: $\Delta \approx 2r_b$.

Figure 27c and 27d are supposed to illustrate this difference in extent by showing the correlation function computed via:

$$f(r) = \sum_{|r_i - r_j| \in [r, r + \Delta]} P_i P_j \quad (9.1)$$

While the ground state covers only a small area, the eigenstate for higher energy is completely distributed over the plane, leading to the question of what the impacts are on the extent of the eigenstates.

In the following we take a closer look at the participation ratio of eigenstates, belonging to different eigenvalues and densities, as well as computing the spectral density and the level spacings.

9.1 Participation ratio

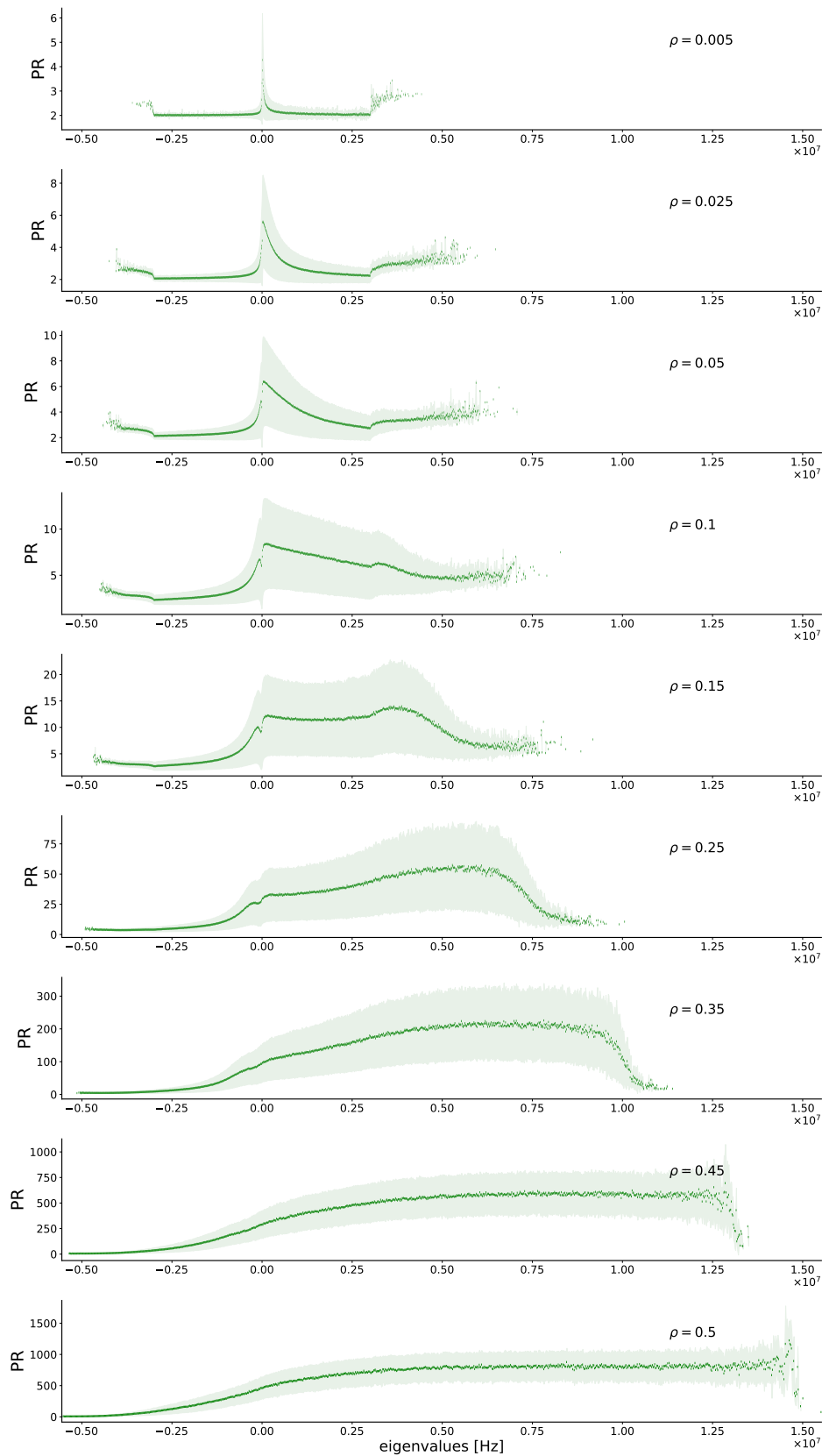


Figure 28: Participation ratio of the energy eigenstates for the respective energy eigenvalues. The plots show an increasing density in a descending order. The x-axis is the same for all the plots allowing comparison. The histogram was not normed to 1, meaning the area under the curve equals the number of eigenstates.

Density	0,005	0,01	0,025	0,05	0,1	0,15	0,2	0,25	0,3	0,35	0,4	0,45	0,5
$\mathcal{R} : 500\mu m$													
Atoms	50	100	250	500	1000	1500	2000	2500	3000	3500	4000	4500	5000
# Avg	50000	40000	30000	15000	7000	3000	1500	1000	800	600	400	250	120

Table 2: For all calculations in this chapter, we used the third measurement series from table 1, shown again in this table.

We calculated the participation ratio for every eigenstate of a particular system. This was done for multiple disorder realizations belonging to the same density. In the end the PRs were averaged over binned eigenvalues in different energy windows.

We made use of two different methods to vary the density. In the first one we changed the number of atoms at fixed system size \mathcal{R} according to table 2. Consequently we obtained for a low number of atoms less eigenstates, than for a system with lots of atoms. To avoid possible bias due to changing atom number, the same calculation of the PR was done for a measurement series, where we varied the system size but fixed the number of atoms. In that way we obtained for every density the same number of eigenstates.

Interestingly, after binning and normalizing, there was no difference in the curves of the PR using those two methods. This indicates among others, that all the eigenvalues of the system with many atoms are in the same range like the eigenvalues of the system with only few atoms. Due to the equality of the methods, we choose to vary the number of atoms for further studies. Therefore all the following results, including the PR in figure 28, were calculated with the systems shown in table 2.

Considering now again the participation ratio shown in figure 28, it appears to exist a mobility edge for eigenvalues at zero for intermediate densities. A mobility edge characterizes the transition between localized and extended states. In our case it is indicated by the abrupt increase of the PR for eigenvalues at 0. However, in case of $\rho = 0.005$ the highest obtained PR is 6, i.e. the states for eigenvalues at zero are still localized. Therefore one cannot speak of a mobility edge at low densities, since all states are localized. In addition, one expects the ground state to be one of the most localized ones, but for small densities the PR starts to rise for lower energies (and for higher energies too). Moreover, we note that especially for $\rho = 0.005$ the PR looks symmetric around $E = 0$.

What is striking as well is, that the minimum of the participation ratios is not at one, like would be expected for a completely localized state. It seems to lie around two. So every eigenstates covers at least two sites. We argue that this is basically caused by the fact, that we simulate the dynamics by setting all on-site energies to zero and working only with interaction parts of the Hamiltonian. In the following we explain further.

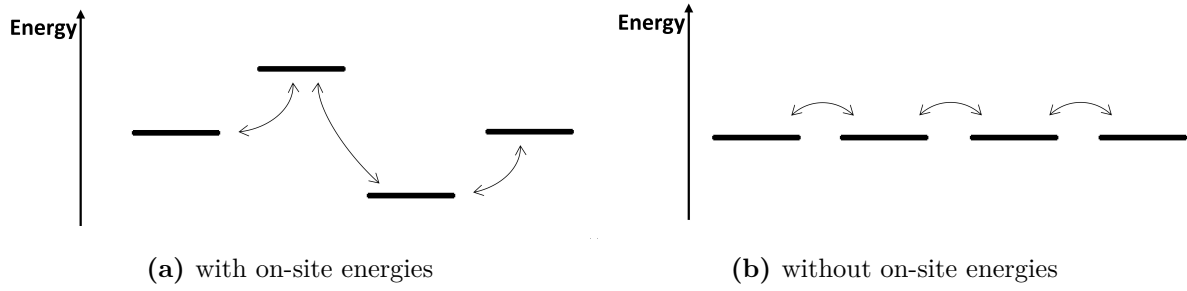


Figure 29: In (a) energy levels of a system with atomic and interaction part are shown. In (b) energy levels of a system with only interactions are shown.

In a system where we have various on-site energies like in figure 29a, one can identify a ground state, which only lives on one site. But in our case (figure 29b) on-site energies originate just due to interaction between two sites. Consequently a ground state consists of several coupled sites, while the other levels are shifted away caused by the interaction. Despite of that, it is still possible to receive a ground state covering only one site. If an eigenstate is localized on a single site, then its energy is zero, because the Hamiltonian only has off-diagonal terms. Thus states with energies significantly different from zero, in particular the ones with low energy, cannot be localized on a single site. In our case, this may actually happen sometimes for low density, if an atom is really "isolated" from the rest of the cloud. This would be the scenario generated manually in figure 7a, where we explained a dressed state.

But in general we think, that the existence of such a arrangement of atoms is much less likely than the existence of a ground state with two sites, explaining why the PR is at least two.

Comparing now the curves of the PR for increasing density, a clear tendency is recognizable. On the one hand for ascending densities we receive higher energies, which stretches the curve. On the other hand the PR increases for high energies. At the final density $\rho = 0.5$ the eigenstates belonging to low energies are localized, while the higher energies seems to be spread out. This explains the illustrated difference for the ground state and highest state in figure 27.

9.2 Level spacing

Besides the participation ratio, one can investigate eigenstates properties through the distribution of the level spacings $\delta_n = E_{n+1} - E_n$. These are best characterized by the ratio [15]:

$$r_n = \frac{\min(\delta_n, \delta_{n-1})}{\max(\delta_n, \delta_{n-1})} \quad (9.2)$$

Localized states present a Poissonian distribution of r_n with an average $\langle r \rangle_P \approx 0.386$, due to the proliferation of degenerate states located at distant spatial positions [15]. In contrast, extended states form a Wigner-Dyson distribution, caused by level repulsion [25]. This is a fact deduced in random matrix theory, considering a Gaussian orthogonal ensemble (GOE) [15, 25]. We expect for extended states: $\langle r \rangle_{GOE} \approx 0.51$ [15].

We calculate the ratio r_n for all levels and evaluate $\langle r \rangle$ for binned energy windows. This can be seen in figure 30 for the lowest and highest density.

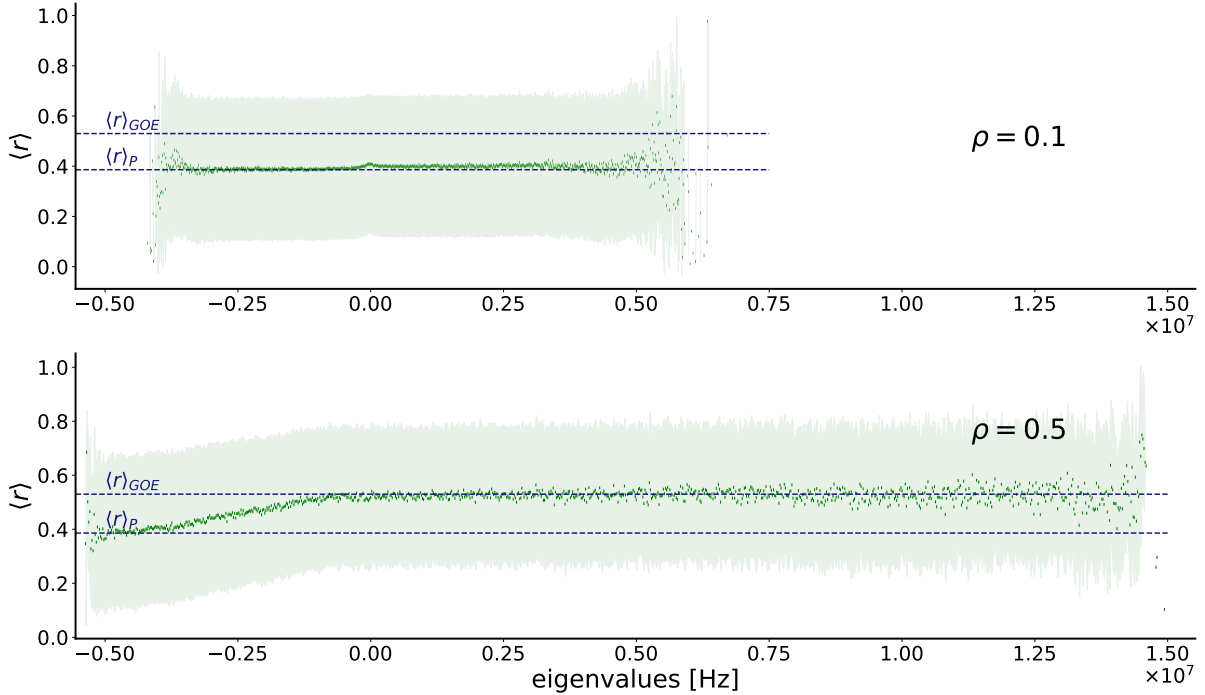


Figure 30: Binned ratio of the level spacings for two different densities

As one can see, the curve for the density $\rho = 0.1$ as well as for $\rho = 0.5$ corresponds to the results received by using the participation ratio in figure 28. In case of a high density $\rho = 0.5$, the ratios $\langle r \rangle$ are approaching to $\langle r \rangle_P$ for low energies, whereas $\langle r \rangle$ equals $\langle r \rangle_{GOE}$ for energies > 0 . This indicates that rather eigenstates belonging to high energies are delocalized. For $\rho = 0.1$ the ratios $\langle r \rangle$ stay at around $\langle r \rangle_P$. Accordingly all eigenstates, independent of the energy, are localized for a small density (high disorder).

In total, the ratio of the level spacings is a suitable method of describing the localization property of the eigenstates.

Figure 31 shown on the next page, represents the dependence of the spectral density on the density of the system. For a low density ρ , the spectral density seems to be perfectly symmetric. Increasing ρ leads to new higher energies, whereas the ground state is almost the same for every density. For rising ρ especially low energies are occupied, whereas their number decreases for higher energies.

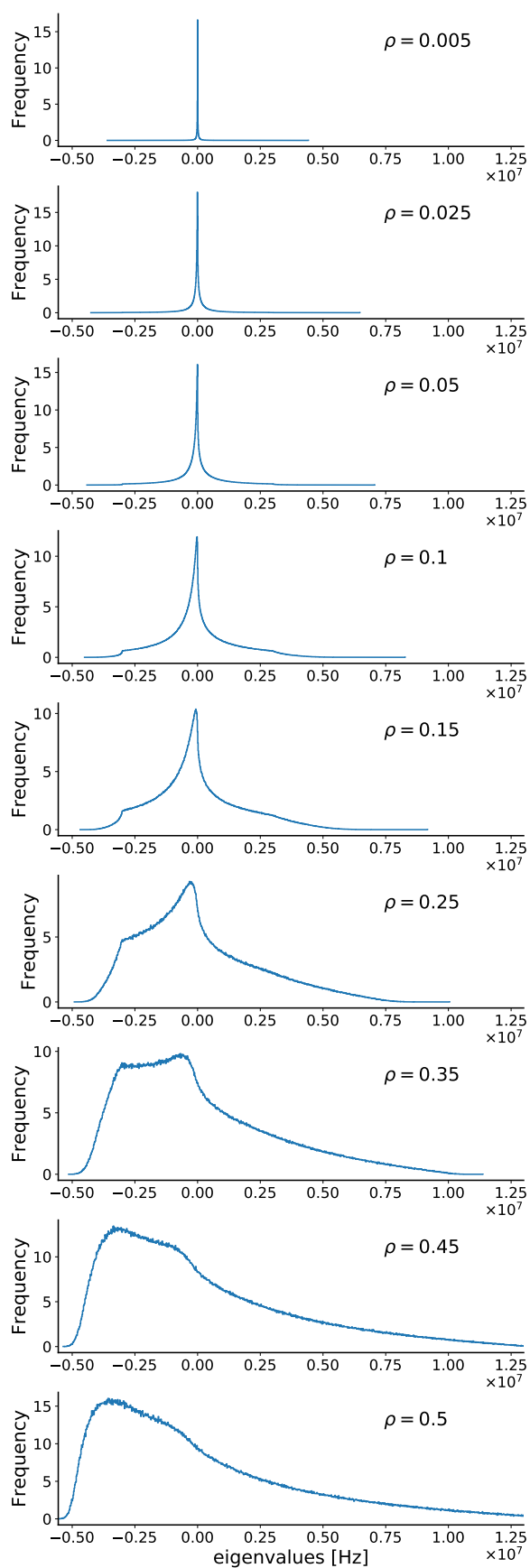


Figure 31: Frequency of the eigenvalues for different densities

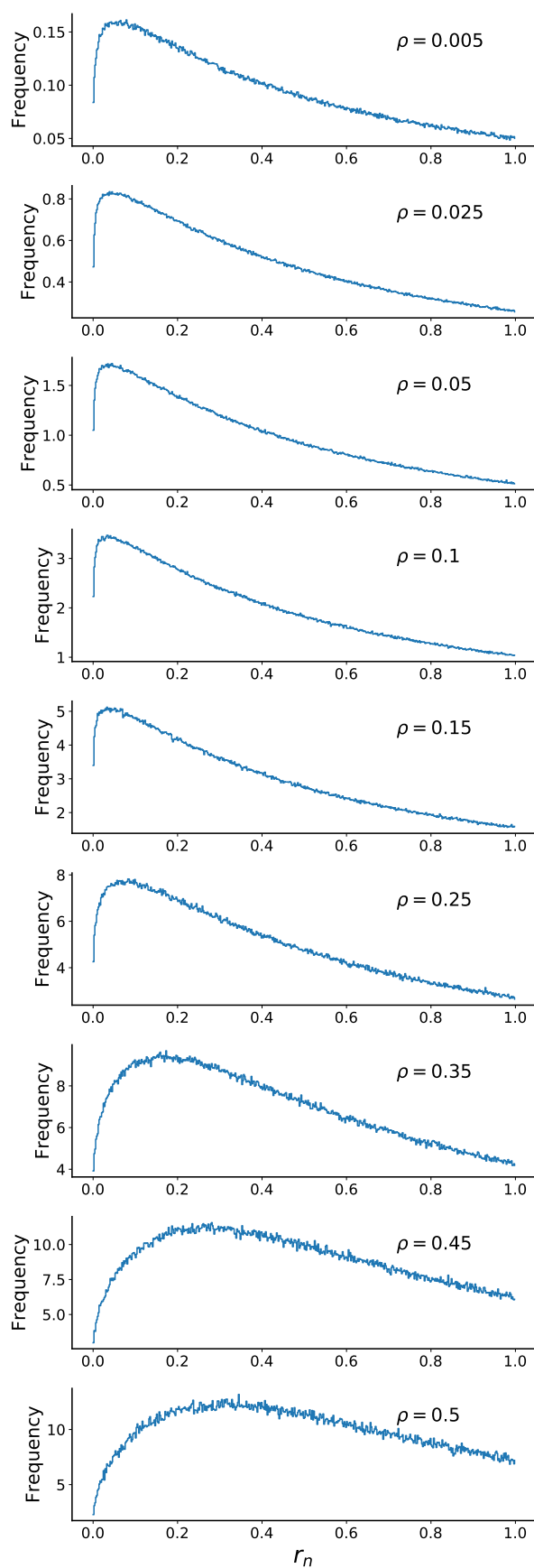


Figure 32: Frequency of the level spacing ratio for different densities

Figure 32 represents the frequency for different r_n . One would expect a Poisson distribution for completely uncorrelated levels [15], which seems to be the case for low densities. By increasing ρ , the level spacing ratios form more and more a curve that looks like a Wigner-Dyson distribution, indicating the increase of extended states. This corresponds to the results, obtained by the participation ratio in figure 28.

We can thus infer, that the level spacings offer a suitable alternative to quantify localization.

Averaging not only over energy intervals, but over all r_n allows us to draw conclusions regarding the scale of delocalization, not only for a single eigenstate, but for the whole system. For a system, where almost all eigenstates are localized, one would expect $\langle r \rangle_{all} \approx \langle r \rangle_P \approx 0.386$, whereas $\langle r \rangle_{all} \approx \langle r \rangle_{GOE} \approx 0.51$ for a system with all eigenstates delocalized [15]. Values between those extrema would indicate a system with mixed localized and delocalized states. We calculated $\langle r \rangle_{all}$ for different system sizes and densities:

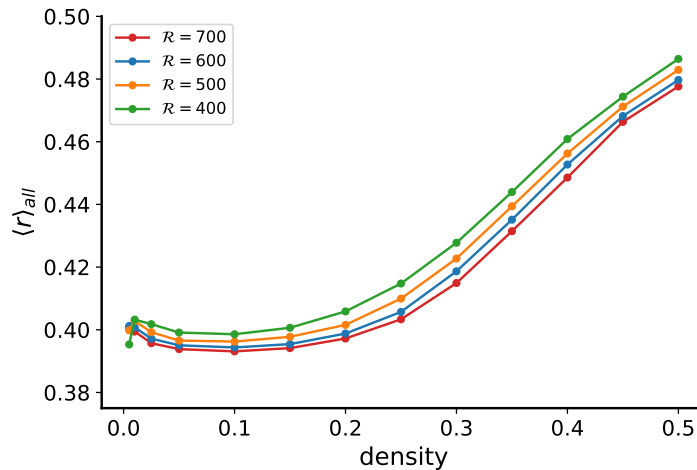


Figure 33: Mean level spacing ratio. The level spacing ratio was averaged over all energies. This was done for different system sizes and different densities, which we already used before, see table 1.

While for low densities almost all eigenstates are localized, the number of delocalized states rises for increasing density. At a density of $\rho = 0.2$, i.e. the critical density after which we fail to observe localization, the ratio of the level spacings starts to rise, indicating a blend between localized and delocalized states. For increasing density the ratio should rise until $\langle r \rangle_{GOE} \approx 0.51$, where every state is delocalized [15].

We note, that the curves for the different system sizes are ordered from the smallest size at the top to the highest at the bottom. There appears to exist a dependence on the number of eigenstates.

Nevertheless, the eigenstates follow the same tendency like the propagation of the single excitation. Decreasing the density (i.e. increasing the randomness) provides localization.

10 Conclusions

We succeeded in implementing a simulation for the propagation of a single spin excitation through a two dimensional frozen Rydberg gas. Especially the time efficiency allows the investigation of a relatively large ensemble of atoms including many time steps. Nevertheless, due to the method of exact diagonalization we are limited to around 10000 atoms. In the end this pays off again, since it makes determining eigenstate properties possible. We started by giving a theoretical derivation of the simulation, followed by an illustration of spin dynamics in the context of small ensembles. The formation of a dressed state could be shown as well as the relevance of the positional placement.

After that, we increased the system size and examined different regimes of transport. In the beginning the excitation started to propagate ballistically with a steady transition, until it resulted in a saturation. No diffusive part could be detected. Additionally we examined the impact of the Rydberg blockade radius. For small r_b the propagation was speed up at the beginning and only for bigger r_b long range transport was assured.

In chapter 8 the effects of Anderson localization were illustrated by firstly showing a qualitative difference between a delocalized propagation for $\rho = 0.5$ and a localized one for $\rho = 0.1$. After making clear, that localization can only be detected if the distribution properties are independent of the system size, we started to investigate the impact of the density on the localization behavior. As was mentioned in the introduction, we were aware that localization has to occur in a 2D system. Therefore the question was not when localization appears, but rather how far it can be detected and how it scales with the density. Accordingly we were able to prove localization effects below a density of $\rho = 0.2$. For higher densities our computing capabilities were not sufficient.

As well as in the case of a random on-site potential, the localization is determined by the magnitude of randomness. One would intuitively expect that a low density constitutes a high randomness and vice versa. In other words not the density, but rather the randomness is the crucial factor. As we were able to prove localization for low densities (i.e. high randomness), our results match the facts of Anderson localization, and its crucial dependence on disorder.

Unfortunately we were not able to provide a functional form describing the dependency of the localization length on the density, as the required exponential decay was not observed.

Finally the eigenstate properties were analyzed. By examining the participation ratio and making use of the level spacings, the difference in the extent of eigenstates for different energies as well as for different system densities was shown. In principle eigenstates belonging to low energies are localized regardless of the density, whereas the extent of states belonging to higher energies depends on ρ .

By means of the averaged ratio of the level spacings a clear trend was noticeable regarding

the degree of localization: Increasing the density leads to a growing number of delocalized eigenstates.

Altogether this thesis was supposed to provide an insight into spin dynamics based on dipole-dipole interaction, resulting in quite interesting phenomena like the Anderson localization. Among others aspects, we hope that the propagation of a single excitation, as well as the impact of disorder on localization effects, has become clearer through this work.

11 Outlook

We want to provide some ideas, which we would have carried out, if time had not been such a limiting factor.

The knowledge that every excitation has to be localized in two dimensions reduces possible surprises. It would be quite interesting to expand the numerical approach to the localization problem to three dimensions. In 3D localization effects don't need to exist. Therefore the mobility edge, which separates a normal diffusion process from localization behavior, could be investigated. Additionally one could change the assumption for the placements of the atoms. Neglecting a fixed radial density, more similarities to the experiment can be achieved by assuming a Gaussian distribution of the atoms.

Improvements of our procedure include for example increasing the number of measured data in the interval, where we proved localization, and where we don't have rescaling effects. Therewith we probably could determine more precisely the scaling behavior of the localization effects depending on the density.

As was already mentioned, the highest density, achievable with random placement, lies around $\rho \approx 0.5$. We could increase the possible density by using a lattice with randomly placed vacancies. This would allow increasing the density further, without dropping the issue of randomness.

Another aspect one could study, is taking on-site energies into account. It is possible to generate this kind of disorder by hand, but it would be quite interesting introducing a term $\sum S_i^z S_j^z$. By expanding the dipolar XY spin Hamiltonian with this term the on-site disorder will be generated by the arrangements of the atoms. Consequently the random placement of atoms leads to random disorder on the diagonal. Thus we would have another factor of randomness.

In the end, the most attractive idea is to develop our simulation by leaving the concept of a single excitation behind, and going to multiple excitations.

Acknowledgements

At this point, I want to thank everybody, who has been supporting me in the last couple of month.

Foremost I would like to thank my supervisor, Martin Gärttner, for giving me the opportunity of completing this thesis under his guidance. I would also like to thank him, as well as the group around him, for the valuable feedback, discussions and much cherished conversations we had, during the last couple of months.

Furthermore thanks goes out Frederick del Pozo for his valuable input, that helped me with proofreading and formulation. Of course my bachelor buddy Fabian Zhou (that short?) shouldn't be missing either.

Last but not least, I also want to thank my family, my friends, and my partner Marina, for supporting me over the last months.

References

- [1] N.Xin J.Guan C.Zhou X.Chen C.Gu Y.Li M.Ratner A.Nitzan J.Stoddart X.Guo, *Concepts in the design and engineering of single-molecule electronic devices*. Nature Reviews Physics volume 1, 211–230, (2019).
- [2] H.Song M.Reed T.Lee, *Single Molecule Electronic Devices*. Adv. Mater. 2011, 23, 1583–1608, (2011).
- [3] A.Orioli A.Signoles H.Wildhagen G.Günter J.Berges S.Whitlock M.Weidemüller, *Relaxation of an isolated dipolar-interacting Rydberg quantum spin system* . arXiv:1703.05957, (2018).
- [4] D.Comparat and P.Pillet, *Dipole blockade in a cold Rydberg atomic sample* . arXiv:1006.0742, (2010).
- [5] K.Hess, *Excitation Transfer in Ultracold Rydberg Atoms*. Masterthesis Freiburg, (2018).
- [6] B.Sun and F.Robicheaux, *Spectral Line Width Broadening from Pair Fluctuation in a Frozen Rydberg Gas*. arXiv:0910.1771, (2009).
- [7] T.Scholak T.Wellens A.Buchleitner, *The Spectral Backbone of Excitation Transport in Ultra-Cold Rydberg Gases*. arXiv:1409.5625v2, (2014).
- [8] C.Hofmann G.Günter H.Schempp N.Müller A.Faber H.Busche M.Robert-de-Saint-Vincent S.Whitlock M.Weidemüller, *An experimental approach for investigating many-body phenomena in Rydberg-interacting quantum systems*. arXiv:1307.1074, (2013).
- [9] J.Cantin T.Xu R.Krems, *The effect of anisotropy of long-range hopping on localization in three-dimensional lattices*. arXiv:1604.01493, (2018).
- [10] P.W.Anderson, *Absence of Diffusion in Certain Random Lattices*. Phys. Rev. 109, 1492, (1958).
- [11] P.Markoš, *Absence of diffusion in certain random lattices: Numerical evidence*. arXiv:0807.2531, (2009).
- [12] F. Wegner, *The mobility edge problem: Continuous symmetry and a conjecture*. Phys. B 25, 327, (1979).
- [13] E.Abrahams P.W.Anderson D.Licciardello T.Ramakrishnan, *Scaling Theory of Localization: Absence of Quantum Diffusion in Two Dimensions*. Phys. Rev. Lett. 42, 673, (1979).
- [14] X.Deng V.Kravtsov G.Shlyapnikov L.Santos, *Duality in power-law localization in disordered one-dimensional systems*. arXiv:1706.04088v4, (2018).
- [15] X.Deng B.Altshuler G.Shlyapnikov L.Santos, *Quantum Levy flights and multifractality of dipolar excitations in a random system*. arXiv:1604.03820v1, (2016).
- [16] S.Datta, *Visualizing Anderson Localization in 3d using Monte Carlo method* . arXiv:1110.6716v5, (2014).
- [17] D.Hundertmark, *A Short Introduction to Anderson Localization* . ResearchGate: Analysis, Stochastics of Growth Processes, and Interface Models, (2019).
- [18] C.Müller D.Delande, *Disorder and interference: localization phenomena* . arXiv:1005.0915v3, (2016).

-
- [19] F.Robicheaux N.Gill, *Effect of random positions for coherent dipole transport*. PHYSICAL REVIEW A 89, 053429, (2014).
 - [20] T.Xu and R.Krems, *Quantum walk and Anderson localization of rotational excitations in disordered ensembles of polar molecules*. New J. Phys. 17 065014, (2015).
 - [21] D.Ben-Avraham D.Havlin, *Diffusion and Reactions in Fractals and Disordered Systems*. Cambridge University Press, (2000).
 - [22] C.Müller, *Spin transport*. MPIPKS Dresden, (2005).
 - [23] M.Calixto E.Romera, *Inverse participation ratio and localization in topological insulator phase transitions*. arXiv:1610.03696v1, (2016).
 - [24] S.Barnett P.Radmore, *Methods in theoretical quantum optics*. Oxford: Clarendon Press, (2005).
 - [25] P.Cizeau and J.P.Bouchaud, *Theory of Lévy matrices*. Phys. Rev. E 50, 1810, (1994).

Eidesstattliche Erklärung

Ich versichere, dass ich diese Arbeit selbstständig verfasst und keine anderen als die angegebenen Quellen und Hilfsmittel benutzt habe.

Unterschrift :

Ort, Datum :